10-6-2020

TGFβR-SMAD3 signaling induces resistance to PARP inhibitors in the bone marrow microenvironment

Bac Viet Le

Juo-Chin Yao

Grant A Challen

Daniel Link

et al

Cell Reports

Article

TGFβR-SMAD3 Signaling Induces Resistance to PARP Inhibitors in the Bone Marrow Microenvironment

Graphical Abstract

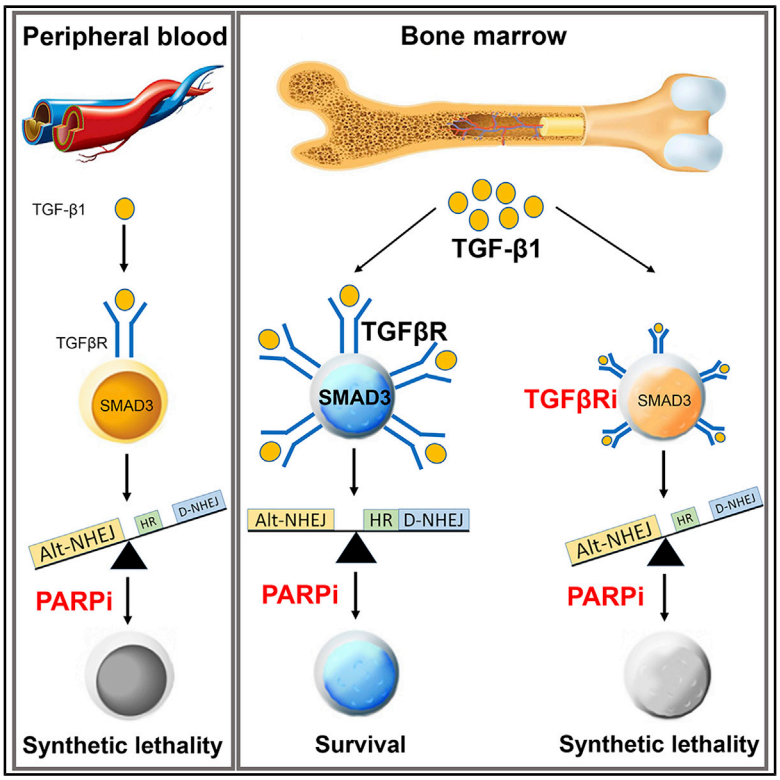

Highlights

- Bone marrow microenvironment (BMM) facilitates DSB repair activity in leukemia cells
- BMM protects leukemia cells from PARP inhibitor (PARPi)-induced synthetic lethality
- TGF-β1-TGFβR kinase-SMAD3 pathway is responsible for PARPi resistance
- Sensitivity of leukemia cells to PARPi is restored by the targeting of the TGF-β1 axis

Authors

Bac Viet Le, Paulina Podszywalow-Bartnicka, Silvia Maifrede, ..., Mariusz A. Wasik, Katarzyna Piwocka, Tomasz Skorski

Correspondence

k.piwocka@nencki.edu.pl (K.P.), tskorski@temple.edu (T.S.)

In Brief

Le et al. show that the TGF-β1-TGFβR kinase-SMAD3 pathway protects leukemia cells from PARP inhibitor (PARPi)-mediated synthetic lethality in the bone marrow microenvironment. The targeting of the TGF-β1 axis restored the sensitivity of leukemia cells to PARPi and prolonged survival of leukemia-bearing mice.

Le et al., 2020, Cell Reports *33*, 108221
October 6, 2020
https://doi.org/10.1016/j.celrep.2020.108221

CellPress

Cell Reports

CellPress
OPEN ACCESS

Article

TGFβR-SMAD3 Signaling Induces Resistance to PARP Inhibitors in the Bone Marrow Microenvironment

Bac Viet Le,[1,2] Paulina Podszywalow-Bartnicka,[2] Silvia Maifrede,[1] Katherine Sullivan-Reed,[1] Margaret Nieborowska-Skorska,[1] Konstantin Golovine,[1] Juo-Chin Yao,[3] Reza Nejati,[4] Kathy Q. Cai,[4] Lisa Beatrice Caruso,[5] Julian Swatler,[2] Michal Dabrowski,[6] Zhaorui Lian,[7] Peter Valent,[8] Elisabeth M. Paietta,[9] Ross L. Levine,[10] Hugo F. Fernandez,[11] Martin S. Tallman,[10] Mark R. Litzow,[12] Jian Huang,[7] Grant A. Challen,[3] Daniel Link,[3] Italo Tempera,[5] Mariusz A. Wasik,[4] Katarzyna Piwocka,[2,*] and Tomasz Skorski[1,13,*]

[1]Sol Sherry Thrombosis Research Center and Fels Institute for Cancer Research and Molecular Biology, Lewis Katz School of Medicine at Temple University, Philadelphia, PA, USA
[2]Nencki Institute of Experimental Biology, Polish Academy of Sciences, Laboratory of Cytometry, Warsaw, Poland
[3]Division of Oncology, Department of Medicine, Washington University School of Medicine, St. Louis, MO, USA
[4]Department of Pathology, Fox Chase Cancer Center, Philadelphia, PA, USA
[5]Fels Institute for Cancer Research and Molecular Biology, Lewis Katz School of Medicine at Temple University, Philadelphia, PA, USA
[6]Nencki Institute of Experimental Biology, Polish Academy of Sciences, Laboratory of Bioinformatics, Warsaw, Poland
[7]Department of Pathology and Laboratory Medicine, Lewis Katz School of Medicine at Temple University, Philadelphia, PA, USA
[8]Department of Internal Medicine I, Division of Hematology and Hemostaseology, Medical University of Vienna and Ludwig-Boltzmann Institute for Hematology and Oncology, Vienna, Austria
[9]Albert Einstein College of Medicine-Montefiore Medical Center, Bronx, NY, USA
[10]Center for Hematologic Malignancies, Memorial Sloan Kettering Cancer Center, New York, NY, USA
[11]Moffitt Malignant Hematology & Cellular Therapy at Memorial Healthcare System, Pembroke Pines, FL, USA
[12]Division of Hematology, Department of Internal Medicine, Mayo Clinic, Rochester, MN, USA
[13]Lead Contact
*Correspondence: k.piwocka@nencki.edu.pl (K.P.), tskorski@temple.edu (T.S.)
https://doi.org/10.1016/j.celrep.2020.108221

SUMMARY

Synthetic lethality triggered by PARP inhibitor (PARPi) yields promising therapeutic results. Unfortunately, tumor cells acquire PARPi resistance, which is usually associated with the restoration of homologous recombination, loss of PARP1 expression, and/or loss of DNA double-strand break (DSB) end resection regulation. Here, we identify a constitutive mechanism of resistance to PARPi. We report that the bone marrow microenvironment (BMM) facilitates DSB repair activity in leukemia cells to protect them against PARPi-mediated synthetic lethality. This effect depends on the hypoxia-induced overexpression of transforming growth factor beta receptor (TGFβR) kinase on malignant cells, which is activated by bone marrow stromal cells-derived transforming growth factor beta 1 (TGF-β1). Genetic and/or pharmacological targeting of the TGF-β1-TGFβR kinase axis results in the restoration of the sensitivity of malignant cells to PARPi in BMM and prolongs the survival of leukemia-bearing mice. Our finding may lead to the therapeutic application of the TGFβR inhibitor in patients receiving PARPis.

INTRODUCTION

Oncogenic tyrosine kinases (OTKs) are found in many types of tumors, including hematologic malignancies (Blume-Jensen and Hunter, 2001; Scheijen and Griffin, 2002). For example, activating mutations of FLT3 cell membrane tyrosine kinase (e.g., FLT3[ITD/TKD]), of ABL1 cytoplasmic/nuclear tyrosine kinase (e.g., BCR-ABL1), and of JAK2 cytoplasmic tyrosine kinase (e.g., JAK2[V617F]) play a pathogenic role in acute myeloid leukemias (AMLs), chronic myeloid leukemia (CML), and myeloproliferative neoplasms (MPNs), respectively. The standard treatment for these malignancies typically uses selective tyrosine kinase inhibitor (TKis) such as quizartinib for FLT3(ITD/TKD) (Larrosa-Garcia and Baer, 2017), imatinib for BCR-ABL1 (Khorashad and Deininger, 2011), and ruxolitinib for JAK2(V617F) (Passamonti and Maffioli, 2018), and/or chemotherapy (cytosine arabinoside in combination with anthracyclines). However, with the exception of CML in chronic phase (CML-CP), complete remissions are rare, and after the initial response, the diseases invariably progress, often becoming more malignant (Shimada, 2019). In addition, a subset of CML-CP patients does not respond favorably to TKi, eventually experiencing progression to a fatal blast phase CML (CML-BP) (Perrotti et al., 2010). Therefore, there is a clear need for additional therapies to improve therapeutic outcomes in patients with OTK-driven leukemias.

Previous reports (Chen et al., 2014; Marty et al., 2013; Sallmyr et al., 2008), including our own (Bolton-Gillespie et al., 2013; Maifrede et al., 2018; Nieborowska-Skorska et al., 2012, 2017a)

indicated that the OTK$^+$ malignant cells accumulate high numbers of spontaneous and drug-induced DNA double-strand breaks (DSBs) in comparison to normal cells, but they manage to survive because of their enhanced/altered ability to repair these breaks. DSBs, the most lethal DNA lesions, are repaired by two major mechanisms, homologous recombination (HR; key effector proteins: BRCA1, BRCA2, CtIP, and RAD51) and DNA-protein kinase (DNA-PK)-mediated non-homologous end-joining (D-NHEJ; key effector proteins: 53BP1, DNA-PKcs, KU70, KU80, and LIG4) (Figure S1) (Chapman et al., 2012). Both HR and D-NHEJ repair DSBs in proliferating cells, while D-NHEJ plays a major role in quiescent cells. Poly (ADP-ribose) polymerase 1 (PARP1)-dependent alternative NHEJ (Alt-NHEJ; key effector proteins: PARP1 and LIG3) serves as backup in both proliferating and quiescent cells (Feng et al., 2011; Karanam et al., 2012). The existence of these redundant pathways creates the opportunity to use a phenomenon called "synthetic lethality," which was originally applied to eliminate cancer cells with mutations in *BRCA1* and *BRCA2* by PARP inhibitor (PARPi) (Bryant et al., 2005; Farmer et al., 2005; Yap et al., 2011).

Although *BRCA1/2* mutations are rare in hematological malignancies (Roy et al., 2011), we and other researchers identified myeloid and lymphoid malignancies displaying specific defects in DSB repair, which are susceptible to synthetic lethality triggered by PARPi (Cimmino et al., 2017; Esposito et al., 2015; Maifrede et al., 2017, 2018; Molenaar et al., 2018; Nieborowska-Skorska et al., 2017a, 2017b; Piao et al., 2017; Podszywalow-Bartnicka et al., 2014; Tobin et al., 2013). In addition, we discovered that the TKi-mediated inhibition of FLT3(ITD/TKD), JAK2(V617F), and BCR-ABL1 kinases caused the downregulation of key effectors of HR (BRCA1, BRCA2, PALB2 and/or RAD51) and D-NHEJ (LIG4) associated with inhibition of HR and D-NHEJ activities and, consequently, sensitized proliferating and quiescent malignant hematopoietic cells to PARPi-mediated synthetic lethality (Maifrede et al., 2018; Nieborowska-Skorska et al., 2017a, 2017b; Sullivan-Reed et al., 2018). These observations resulted in clinical trials that tested PARPi in patients with hematological malignancies (reviewed in Faraoni et al., 2019).

Since these malignancies usually reside in peripheral blood (PB) and hematopoietic tissues (e.g., bone marrow [BM], spleen), it is of paramount importance to test the effect of PARPi in different microenvironments, especially because the BM microenvironment (BMM) protects leukemia cells against TKi and cytotoxic drugs (Zhou et al., 2016). This effect is associated with the leukemia-mediated remodeling of BMM, which engages various cells and cytokines (e.g., C-X-C motif chemokine 12 [CXCL12] - C-X-C chemokine receptor type 4 [CXCR4] pathway and transforming growth factor beta 1 [TGF-β1] - transforming growth factor beta receptor (TGFβR) kinase signaling) (Brunen et al., 2013; Schelker et al., 2018; Zeng et al., 2009).

We report here that HR and/or D-NHEJ-deficient hematological malignancies, which are sensitive to PARPi-mediated synthetic lethality in conditions mimicking the PB microenvironment (PBM), are resistant to PARPi in conditions mimicking the BMM. We show that TGF-β1 produced by BM stromal cells activates a hypoxia-induced TGFβR kinase-SMAD2/3 pathway in leukemic cells to promote DSB repair. Genetic and pharmacological inhibition of TGFβR kinase and SMAD3 reduced DSB repair and restored the sensitivity of leukemic cells to PARPi in the BMM, suggesting potential clinical applications of TGFβR kinase inhibitors in PARPi-mediated therapies.

RESULTS

BMM Protects Hematological Malignant Cells against PARPis

To test the impact of the BMM on PARPi-mediated synthetic lethality, previously identified BRCA1/2 pathway-deficient leukemias (e.g., BCR-ABL1 BRCA1-deficient CML, AML1-ETOBRCA2-deficient AMLs, and BRCA1/2-deficient AMLs; Esposito et al., 2015; Nieborowska-Skorska et al., 2017b; Podszywalow-Bartnicka et al., 2014), and FLT3(ITD);*TET2mut* AMLs and JAK2(V617F);*TET2mut* MPNs (TET2mut was associated with BRCA1 deficiency and enhanced sensitivity to DNA-damaging agents; Chen et al., 2018) were incubated in conditions mimicking the BMM and PBM with PARPi olaparib and talazoparib (Figure 1A). Autologous and allogeneic BM stromal cells and stromal cell-derived cell lines (human HS-5 and murine OP9) were used to create stromal monolayers, as indicated.

The results of clonogenic tests clearly showed that when compared to the PBM, the BMM-dc protected human and murine malignant cells from the toxic effect of PARPi, whereas normal cells were resistant to PARPi in both the PBM and BMM (Figures 1B and 1C). Since the protective effect of the BMM was sustained when human and murine malignant cells were separated from stroma cells by 0.4 μm polyethylene terephthalate (PET) cell culture insert (BMM-idc) and was also observed using stromal cell conditioned medium (BMM-cm), we concluded that cell-cell contact and extracellular vesicles were not involved (Figure 1D). Moreover, BMM-direct contact (dc) also protected Lin$^-$CD34$^+$CD38$^-$CFSE^{max} quiescent malignant hematopoietic stem cells from the toxic effect of PARPi olaparib in a malignant cell-stromal cell contact-independent manner (Figure 1E).

TGF-β1-TGFβR Signaling in the BMM Causes Resistance to PARPis

The results in Figure 1 implicated cytokine-dependent resistance to PARPi in the BMM. Hematologic malignancies induce extensive "remodeling" of the BM niche, which involves numerous cytokines, including CXCL12 and TGF-β1 (Schepers et al., 2015; Tabe and Konopleva, 2017).

TGFβR1 inhibitor SB431542 and TGF-β1 neutralizing antibody 1D11 sensitized human FLT3(ITD);*TET2mut* and/or murine FLT3(ITD);*Tet2*$^{-/-}$ leukemia cells to PARPi olaparib and TKi quizartinib in BMM (Figure S2). However, inhibitors of the CXCL12-CXCR4 pathway (CXCR4i AMD3100 and CXCR4 antagonist WZ811) sensitized leukemia cells to quizartinib, but they did not affect the response to olaparib. Therefore, these results suggest the key role of the TGF-β1-TGFβR pathway in the resistance to PARPi in the BMM.

TGF-β1, a major cytokine involved in the leukemic BM niche remodeling process, is produced by BM stromal cells (Duan et al., 2014; Krause et al., 2013). We confirmed that TGF-β1

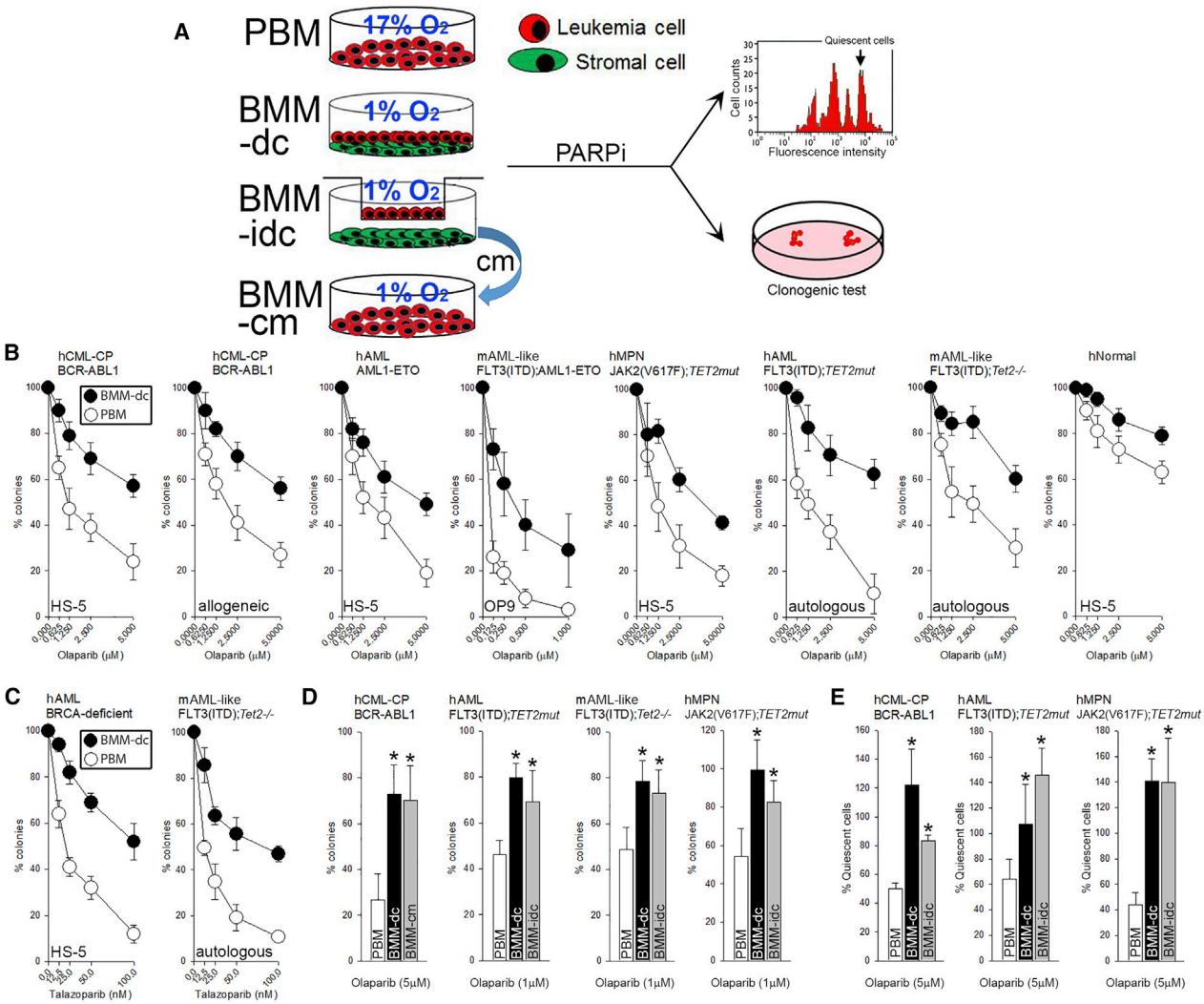

Figure 1. BMM Protects BRCA-Deficient Leukemia Cells from PARPi-Mediated Toxicity

(A) Experimental scheme. PBM, peripheral blood microenvironment mimicking conditions; BMM, bone marrow microenvironment mimicking conditions, dc, direct contact; idc, indirect contact; cm, conditioned medium.

(B and C) Clonogenic activity of Lin$^-$CD34$^+$ human (h) and Lin$^-$cKit$^+$ murine (m) malignant hematopoietic cells expressing indicated oncogenes (n = 3–4 donors [patients or mice]/group) and normal human hematopoietic cells (n = 3 healthy donors) after treatment with olaparib (B) or talazoparib (C) in PBM (white circles) and BMM-dc (black circles); stromal cells are indicated.

(D and E) Lin$^-$CD34$^+$ human and Lin$^-$cKit$^+$ murine malignant hematopoietic cells expressing indicated oncogenes were treated with olaparib in PBM, BMM-dc, BMM-idc, and in BMM-cm; stromal cells are indicated in (B). Results represent mean % ± SDs of (D) colonies and (E) Lin$^-$CD34$^+$CD38$^-$CFSE^{max} quiescent cells (when compared to untreated cells); *$p < 0.05$ when compared to PBM.

was secreted by stromal cells (primary stromal cells and cell lines HS-5 and OP9) in our experimental conditions (Figure S3). TGF-β1-induced oligomerization of TGFβR1 and TGFβR2 subunits causes the activation of TGFβR serine/threonine kinase activity, followed by the phosphorylation of downstream targets—for example, SMAD2 and SMAD3—which oligomerize with SMAD4 to modulate the transcription of the target genes (Heldin and Moustakas, 2016). By using flow cytometry and western analysis we detected a 2- to 3-fold increase in TGFβR1 and TGFβR2 expression in human FLT3(ITD);*TET2mut* Lin$^-$CD34$^+$ primary AML cells and in BCR-ABL1 K562 cells in BMM-dc versus PBM (Figure 2A). This effect was triggered by hypoxia (Figure 2B) and was associated with the enhanced phosphorylation of SMAD2 and SMAD3 (Figure 2C). However, we did not detect an elevated DNA damage response (no increase in phospho-ATM and γ-H2AX was observed), as reported in epithelial cells (Li et al., 2019).

To obtain direct evidence that TGF-β1 → TGFβR signaling regulates sensitivity to PARPi in the BMM, TGFβR2 was deleted by tamoxifen-inducible Cre endonuclease in JAK2(V617F);*Tgfβr2*$^{-/-}$ murine MPN-like cells (Figure 2D, right panels) or downregulated by CRISPR-Cas9 in BCR-ABL1 K562-Cr cells (Figure 2E, inset). Furthermore, TGF-β1 synthesis was reduced by CRISPR-Cas9 in the HS-5-Cr stromal cell line

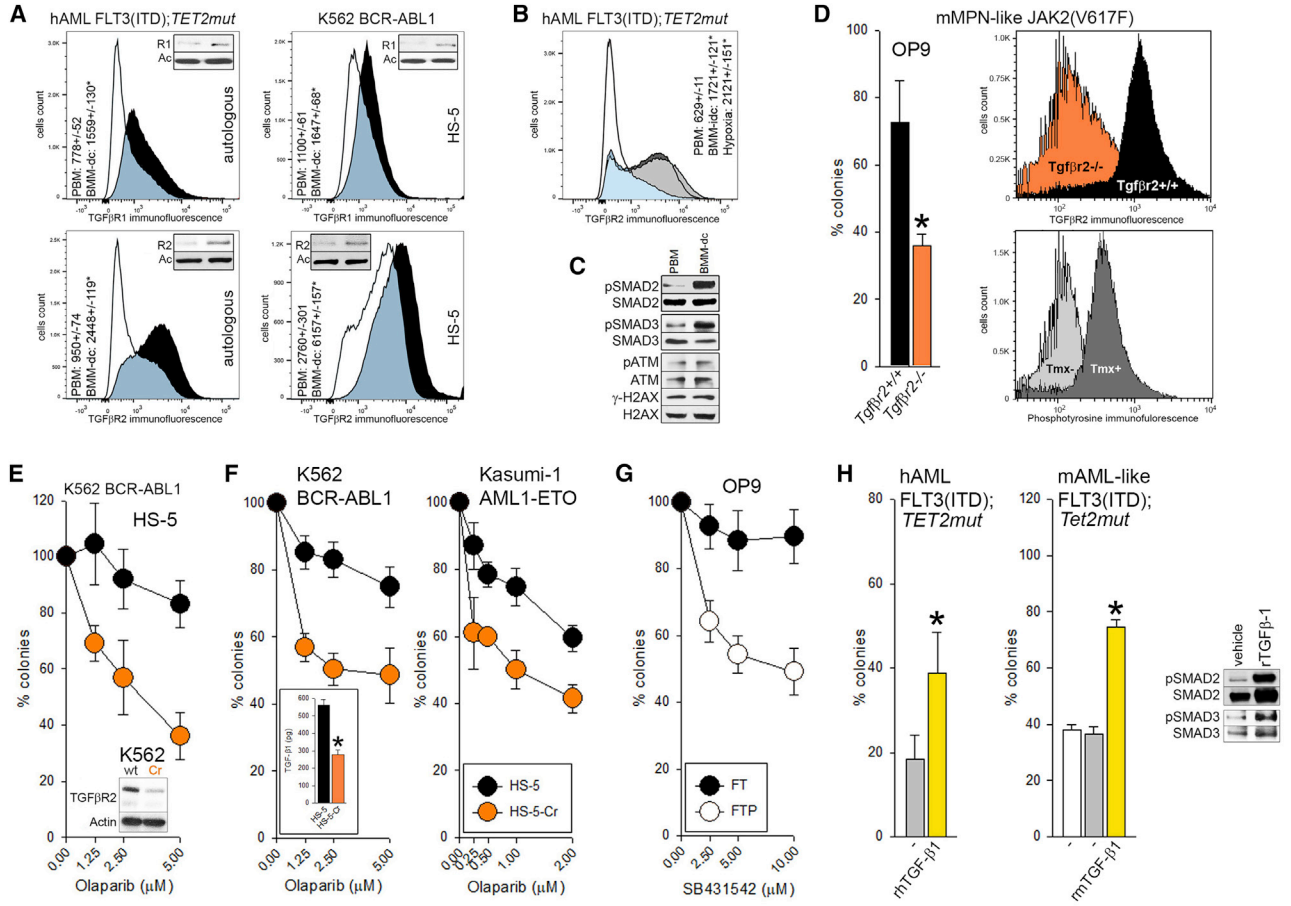

Figure 2. TGF-β1 - TGFβR Kinase Signaling Induced Resistance to PARPi in the BMM

(A and B) TGFβR1 and TGFβR2 expression in human FLT3(ITD);*TET2mut* Lin$^-$CD34$^+$ AML cells (3 patients) and in BCR-ABL1 K562 cells was detected by flow cytometry (diagrams) and by western blot (insets) in (A) PBM (white histograms), BMM-dc (black histograms), and in (B) PBM (white histogram), BMC-idc (dark gray histogram), and PBM + hypoxia (light gray histogram).

(C) Western blots detected indicated proteins in nuclear lysates from human FLT3(ITD);*TET2mut* Lin$^-$CD34$^+$ cells in PBM and BMM-dc.

(D) Sensitivity of JAK2(V617F);*Tgfβr2*$^{-/-}$ and JAK2(V617F);*Tgfβr2*$^{+/+}$ cells to 1 μM olaparib in BMM-dc. Results represent mean % colonies ± SDs when compared to untreated cells; *p < 0.05. Depletion of Tgfβr2 in tamoxifen (Tmx)-treated cells and expression of JAK2(V617F) in Tmx-untreated (–) and -treated (+) cells were validated by immunofluorescence (upper and lower right panels, respectively).

(E) Sensitivity of BCR-ABL1 K562-WT (wild-type) and K562-Cr cells to olaparib in BMM-dc. The results represent mean % colonies ± SDs when compared to untreated cells.

(F) Sensitivity of K562-wt and Kasumi-1 cells to olaparib when cultured in BMM-dc with HS-5 cells and HS-5-Cr cells with the downregulated production of TGF-β1 (inset, left panel). The results represent mean % colonies ± SDs.

(G) Lin$^-$cKit$^+$ murine FLT3(ITD);*Tet2*$^{-/-}$ (FT) and FLT3(ITD);*Tet2*$^{-/-}$;*Parp1*$^{-/-}$ (FTP) cells were treated with the indicated concentrations of SB431542 in BMM-dc conditions followed by plating in methylcellulose. The results represent mean % colonies ± SDs.

(H) Human Lin$^-$CD34$^+$ FLT3(ITD);*TET2mut* AML cells and murine Lin$^-$c-Kit$^+$ FLT3(ITD);*Tet2*$^{-/-}$ cells in hypoxia were treated with 1 μM olaparib in the presence of 3 ng/mL recombinant human TGF-β1 (rhTGF-β1) or recombinant mouse (rmTGF-β1), respectively, (yellow bars) or vehicle (gray bars), or were cultured in normoxia (white bars). The results represent mean % colonies ± SDs; *p < 0.05. Western blots of phospho-SMAD2 (pSMAD2) and SMAD2, and pSMAD3 and SMAD3 in representative nuclear lysates from cells treated with TGF-β1 or vehicle.

See also Figures S2 and S3.

(Figure 2F, left panel inset). The results in Figures 2D–2F clearly show that the deletion of TGFβR2 in hematopoietic malignant cells or the inhibition of TGF-β1 production by stromal cells was associated with the enhanced sensitivity of malignant cells to PARPi olaparib in BMM-dc. In addition, the absence of PARP1 in FLT3(ITD);*Tet2*$^{-/-}$;*Parp1*$^{-/-}$ cells strongly sensitized them to TGFβR1i SB431542 in the BMM-dc (Figure 2G). Conversely, stimulation of the TGFβR kinase pathway by recombinant TGF-β1 in human Lin$^-$CD34$^+$ FLT3(ITD);*TET2mut* cells and murine Lin$^-$c-Kit$^+$ FLT3(ITD);*Tet2*$^{-/-}$ cells in hypoxia (as documented by the enhanced phosphorylation of SMAD2 and SMAD3) induced resistance to olaparib (Figure 2H). These results strongly suggest that the hypoxia-induced overexpression of TGFβR1/2 kinase sensitizes malignant hematopoietic cells to stromal cells-derived TGF-β1 to induce resistance to PARPi in BMM.

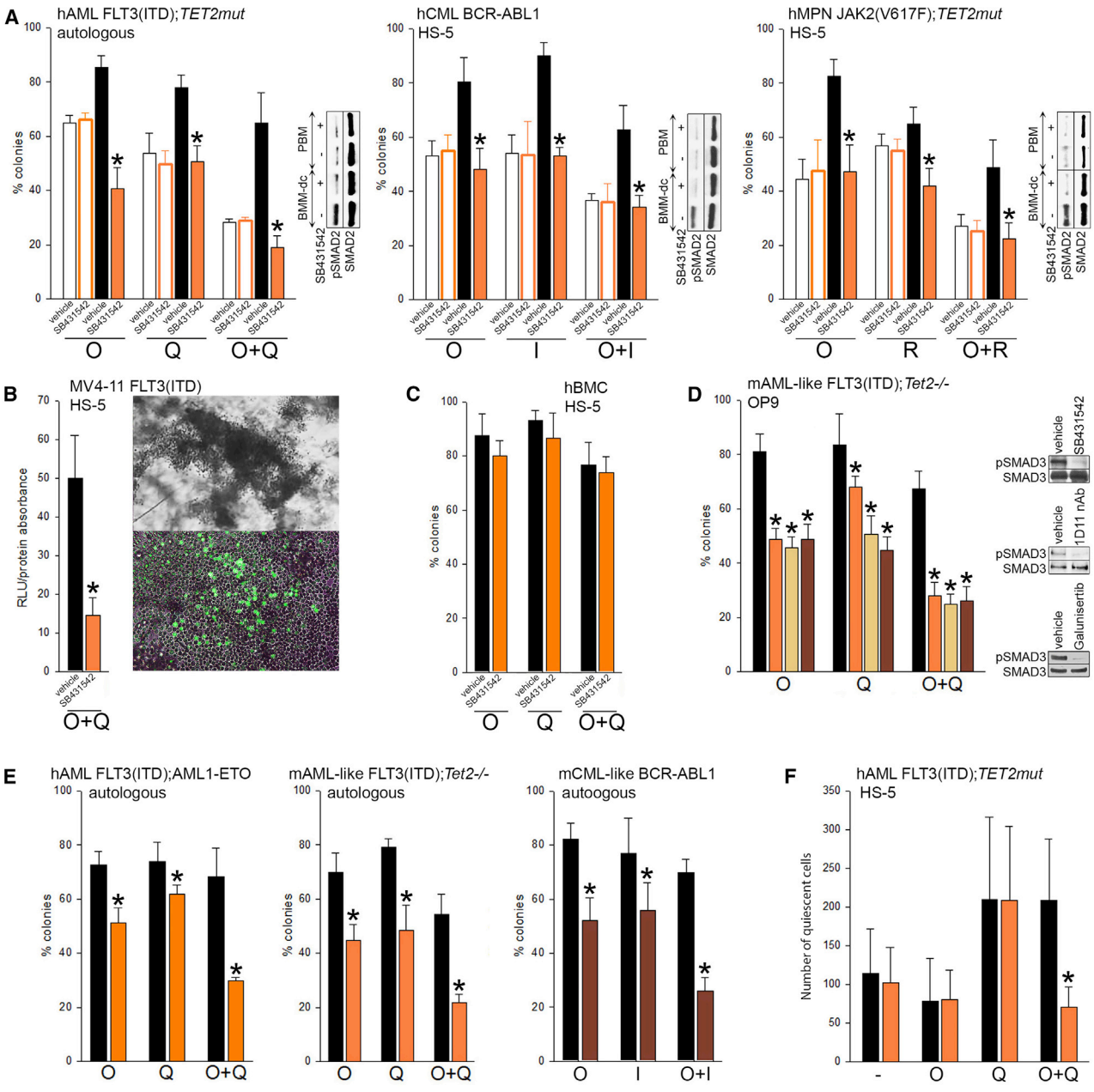

Figure 3. Inhibition of TGF-β1-TGFβR Kinase Signaling Restored the Sensitivity of OTK-positive Cells to TKi+PARPi in the BMM.

(A) Human Lin$^-$CD34$^+$ primary FLT3(ITD);*TET2mut* AML cells (3 patients) and JAK2(V617F);*TET2mut* MPN cells (1 patient), and BCR-ABL1 CML K562 cells were left untreated or were treated with 2.5 μM olaparib (O), 50 nM quizartinib (Q), 25 nM ruxolitinib (R), 1 μM imatinib (I), O + Q, O + R, and O + I in PBM (transparent bars) or BMM-dc (filled bars, stromal cells indicated) in the presence of 10 μM SB431542 or vehicle, as indicated. The results represent mean % colonies ± SDs; *$p < 0.05$ when compared to corresponding black bars. Western blots show pSMAD2 and total SMAD2 in nuclear lysates.

(B) Sensitivity of FLT3(ITD) MV-4-11 AML cells to 50 nM talazoparib + 100 nM quizartinib in the presence of 25 μM SB431542 (orange bar) or vehicle (black bar) in BMM-3d co-culture. The results represent mean relative luminescence units (RLUs) to protein absorbance in the sample ± SD. Upper image, a sphere image taken using bright-field microscope Motic AE20 with objective 4×. Lower image, overlay of bright field and GFP fluorescence (GFP$^+$ cells in green) taken with a Nikon Eclipse Ti microscope with objective 10×.

(C) Clonogenic activity of Lin$^-$CD34$^+$ BM cells from healthy donors (hBMC, 3 donors) treated in BMM-dc with 50 nM quizartinib (Q), 2.5 μM olaparib (O), and Q + O in the presence of 10 μM SB431542 (orange bars) or vehicle (black bars). The results represent mean % colonies ± SDs.

(D) Lin$^-$cKit$^+$ murine FLT3(ITD);*Tet2*$^{-/-}$ AML-like cells (3 mice) were treated in BMM-dc with 100 nM quizartinib (Q), 1 μM olaparib (O), and Q + O in the presence of 10 μM SB431542 (orange bars), 3 ng/mL 1D11 antibody (yellow bars), 10 μM galunisertib (brown bars), or vehicle (black bars). The results represent mean % colonies ± SDs; *$p < 0.05$ when compared to corresponding vehicle-treated cells. Representative western blots of pSMAD3 and SMAD3 in nuclear lysates from cells treated with SB431542, 1D11 antibody, galunisertib, or vehicle.

(legend continued on next page)

Inhibition of TGFβR Kinase Sensitizes Malignant Hematopoietic Cells to PARPi in the BMM

We reported previously that quizartinib-treated FLT3(ITD) cells, ruxolitinib-treated JAK2(V617F) cells, and imatinib-treated BCR-ABL1 cells display "acute" deficiencies in HR and D-NHEJ and were highly sensitive to PARPi-triggered synthetic lethality (Maifrede et al., 2018; Nieborowska-Skorska et al., 2017a, 2017b). In concordance, the combination of TKi (quizartinib, ruxolitinib, imatinib) with PARPi olaparib inhibited the clonogenic activity of human Lin$^-$CD34$^+$ FLT3(ITD);*TET2mut* AML cells, JAK2(V617F);*TET2mut* MPN cells, and BCR-ABL1 CML K562 cells in the PBM, and TGFβRi SB431542 did not alter this effect (Figure 3A). However, in the BMM-dc, cells were resistant to PARPi ± TKi, but the inhibition of TGFβR1 kinase by SB431542 (confirmed by the downregulation of phospho-SMAD2) restored the sensitivity. SB431542 also sensitized FLT3(ITD) MV4-11 AML cells to quizartinib + talazoparib in 3-dimensional BMM co-culture (BMM-3d) with HS-5 cells (Figure 3B). Importantly, SB431542 did not enhance the sensitivity of Lin$^-$CD34$^+$ hematopoietic cells from healthy donors to TKi + PARPi in the BMM-dc (Figure 3C).

Moreover, another TGFβR1i, galunisertib, as well as the TGF-β1 neutralizing antibody 1D11 also restored the sensitivity of murine FLT3(ITD);*Tet2*$^{-/-}$ leukemia cells to olaparib ± quizartinib in BMM-dc (Figure 3D). In addition, we showed that not only stromal cell lines but also autologous stromal cells protected murine and human FLT3(ITD);*Tet2*$^{-/-}$, FLT3(ITD);AML1-ETO, and BCR-ABL1 leukemias against olaparib ± TKi in BMM-dc, and that SB431542 and galunisertib eradicated the protective effect of autologous stroma (Figure 3E).

In concordance with previous reports (Karantanou et al., 2018), the BMM promoted the quiescence of leukemia cells manifested by the accumulation of cells in G0/G1 phase of the cell cycle (Figure S4). Quiescent leukemia stem cells (LSCs) are refractory to TKis and are often responsible for the resistance to therapies and/or disease relapse (Barnes and Melo, 2006; Li and Bhatia, 2011). We demonstrated that the BMM-dc protected FLT3(ITD);*TET2mut* Lin$^-$CD34$^+$CD38$^-$CFSE^{max} quiescent human AML stem cells against olaparib + quizartinib (Figure 3F). Remarkably, quiescent AML stem cells treated with SB431542 re-gained the sensitivity to the combination of these drugs.

TGFβRi Enhances the Anti-Leukemia Effect of PARPi + TKi *In Vivo*

The results presented in Figure 3 imply that TGFβRi should enhance the elimination of leukemia cells from the BM of TKi + PARPi-treated patients. To test this hypothesis, the anti-leukemia effect of TKi (imatinib for BCR-ABL1 and quizartinib for FLT3(ITD) cells) + PARPi (talazoparib) ± TGFβR1i (SB431542) was examined in SCID mice bearing GFP$^+$ BCR-ABL1 CML-like and GFP$^+$ FLT3(ITD);*Tet2*$^{-/-}$ AML-like leukemias (Figure 4A). A short and aggressive 7-day regimen was applied to test the beneficial effects of TGFβRi. SCID mice were used as hosts to exclude the impact of PARPi-mediated immune modulation on the therapeutic effect (Césaire et al., 2018). Talazoparib was used here because it displays better pharmacokinetic parameters in mice than does olaparib (Shen et al., 2013) and was already tested in mice against HR/D-NHEJ-deficient hematological malignancies (Maifrede et al., 2018; Nieborowska-Skorska et al., 2017a, 2017b).

As expected, imatinib + talazoparib and quizartinib + talazoparib exerted anti-leukemia effects in the PB of mice bearing CML-like and AML-like leukemias, respectively, and the addition of SB431542 did not enhance this effect (Figure 4B). Remarkably, while the anti-leukemia effects of the TKi + PARPi combination were quite limited in the BM and spleen, the addition of TGFβRi greatly enhanced this effect. Moreover, TGFβRi prolonged the survival of CML-like and AML-like bearing mice treated with TKi + PARPi (Figure 4C). Importantly, secondary recipients of BM cells harvested at the end of the TKi + PARPi + TGFβRi treatment survived longer than mice injected with cells from TKi + PARPi-treated animals (Figure 4D), suggesting that the addition of TGFβRi to TKi + PARPi targeted LSCs in the BM niche. Immunohistochemical analysis of GFP$^+$ leukemic cells in BM supports the conclusion that TGFβRi enhanced the targeting of CML-like (Figure 4E) and AML-like (Figure 4F) leukemia cells by TKi + PARPi in the BMM.

Inhibition of TGFβR Kinase Induces DSB Repair Defects in Leukemia Cells in the BMM

We observed that the inhibition of the TGFβR kinase by SB431542 was associated with the accumulation of DSBs (detected by neutral comet assay) in olaparib and olaparib + quizartinib-treated FLT3(ITD);*Tet2*$^{-/-}$ murine AML-like cells in BMM-dc (Figure 5A), which coincided with the enhanced sensitivity to PARPi (Figures 2 and 3). However, the measurement of DSBs by the detection of histone 2AX phosphorylated on serine 139 (γ-H2AX) (Bonner et al., 2008) showed less abundant staining in olaparib + quizartinib-treated FLT3(ITD);*Tet2*$^{-/-}$ cells when TGFβR kinase was inhibited by SB431542 (Figure 5B). These results suggest that the ATM and/or ATR kinases-mediated sensing of DSBs may be deregulated upon the inhibition of TGFβR kinase (Bonner et al., 2008).

The impact of TGFβRi on DSB repair (Figure S1) was tested using specific reporter cassettes measuring HR, D-NHEJ, and Alt-NHEJ repair activities (Figure 5C, right panel), as described before (Nieborowska-Skorska et al., 2017b). The treatment with SB431542 caused ~9- and 2-fold reductions of HR and

(E) Lin$^-$CD34$^+$ cells from FLT3(ITD);AML1-ETO AMLs (3 patients), and Lin-cKit$^+$ cells from FLT3(ITD);*Tet2*$^{-/-}$ AML-like mice (3 mice) and BCR-ABL1 CML-like mice (3 mice) were treated in BMM-dc with 100 nM quizartinib (Q), 1 μM imatinib (I), 1 μM olaparib (O), O + I, and O + Q in the presence of 10 μM SB431542 (orange bars), 10 μM galunisetrib (brown bars), or vehicle (black bars). The results represent mean % colonies ± SDs; *$p < 0.05$ when compared to corresponding vehicle-treated cells.

(F) Lin$^-$CD34$^+$ cells from FLT3(ITD);*TET2mut* AML were treated in BMM-dc with 10 nM quizartinib (Q), 1 μM olaparib (O), and O + Q in the presence of 10 μM SB431542 (orange bars) or vehicle (black bars). The results represent the mean number of Lin$^-$CD34$^+$CD38$^-$CFSE^{max} quiescent cells/5 × 10^5 cells ± SD; *$p < 0.05$ when compared to corresponding vehicle-treated cells.

See also Figure S4.

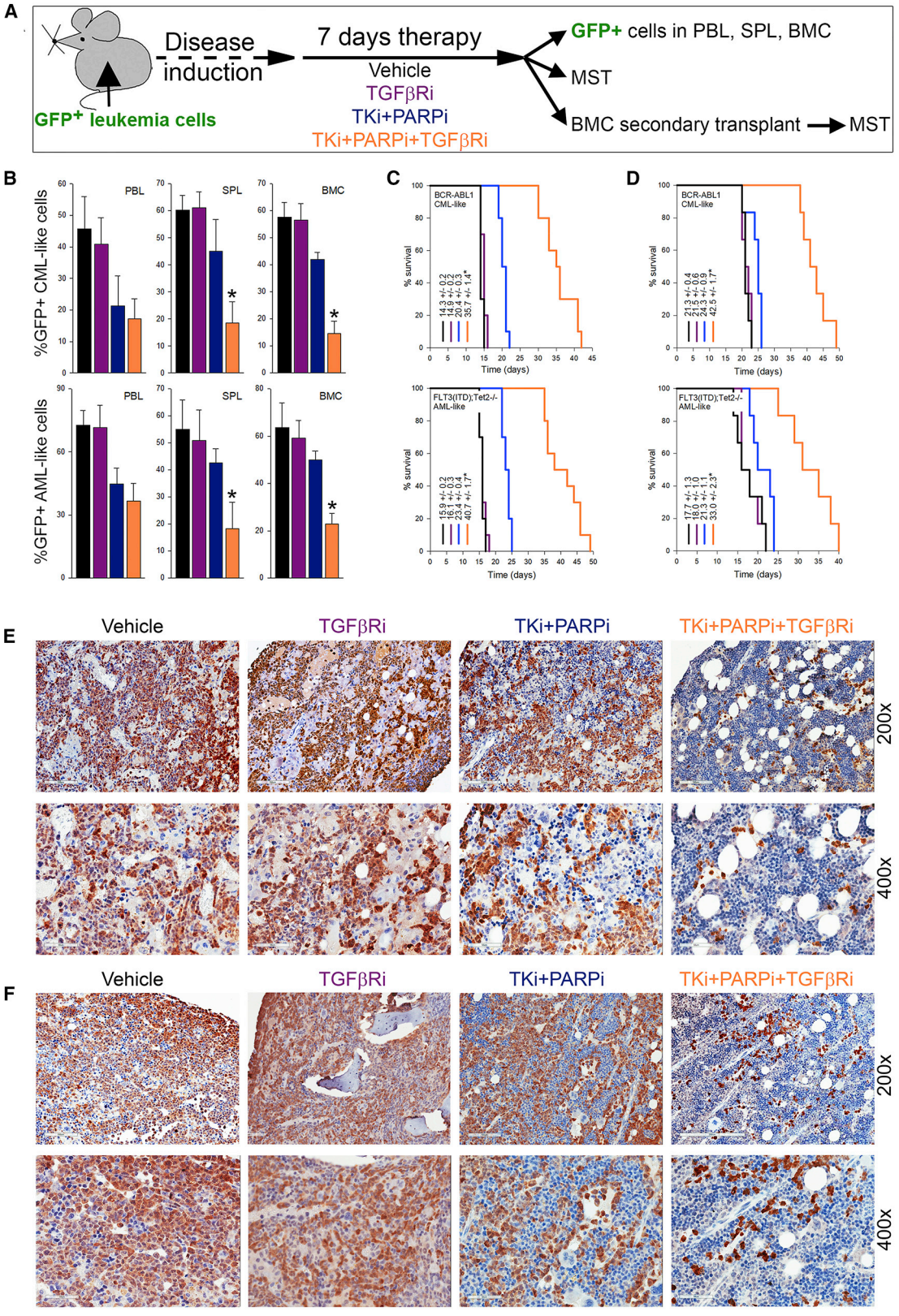

(legend on next page)

D-NHEJ, respectively, whereas Alt-NHEJ was enhanced by ~2-fold (Figure 5C, left panel). Western blot analysis revealed that TGFβRi-mediated modulation of DSB repair was associated with the downregulation of ATM kinase (Figure 5D). In addition, BRCA1 and BRCA2 (HR proteins) and DNA-PKcs and LIG4 (D-NHEJ) proteins were strongly downregulated in FLT3(ITD);*Tet2*$^{-/-}$ AML-like cells in BMM-dc after the inhibition of TGFβR kinase. At the same time, TGFβRi did not affect the expression of Alt-NHEJ proteins (PARP1, LIG3). These TGFβRi-induced changes in DNA damage/repair were not dependent on the cell cycle (Figure S5). ATM, BRCA1, BRCA2, DNA-PKcs, and LIG4 but not Alt-NHEJ proteins were also downregulated in the CML K562-Cr cell line (in which expression of TGFβR2 was reduced by CRISPR-Cas9) maintained in BMM-dc (Figure 5D), confirming the key role of TGFβR kinase-dependent signaling in regulating the DSB repair machinery.

TGFβR-SMAD3 Regulates the Sensitivity of Leukemia Cells to PARPi ± TKi in the BMM

TGFβR kinase activates numerous downstream signaling effectors, including the transcriptionally active SMAD2/3/4 complex and several kinases (e.g., PI3K, RAF1, PAK1, TAK1) (Vander Ark et al., 2018). In addition, miR-182 and miR-183 were implicated in TGF-β1-mediated signaling in cancer (Liu et al., 2018; Zhou et al., 2019).

To identify the downstream mechanisms responsible for TGFβR-mediated resistance to PARPi, murine AML-like FLT3(ITD);*Tet2*$^{-/-}$ cells were treated in BMM-dc conditions with olaparib ± quizartinib in the presence of SMAD3, PI3K, RAF1, PAK1, and TAK1 inhibitors. Remarkably, only the SMAD3 inhibitor (SMAD3i) sensitized leukemia cells to olaparib ± quizartinib (Figure 6A), which was associated with the inhibition of the expression of all five DSB repair genes downregulated also by TGFβRi: *ATM*, *BRCA1*, *BRCA2*, *PRKDC*, and *LIG4* at the mRNA (Figure 6B) and protein (Figure 6C) levels. The PI3K, RAF1, PAK1, and TAK1 inhibitors exerted inhibitory effects only against BRCA1 and/or BRCA2 expression (Figure S6A).

The key role of SMAD3 downstream of TGFβR in triggering PARPi resistance in BMM-dc was validated by showing that the inhibition of the activated phospho-SMAD3 by SMAD3(D407E) dominant-negative mutant restored the sensitivity of FLT3(ITD);*Tet2*$^{-/-}$ AML-like cells to olaparib ± quizartinib (Figure 6D), which was associated with the downregulation of the ATM, BRCA1, BRCA2, DNA-PKcs, and LIG4 proteins (Figure 6E). Interestingly, putative SMAD2/3/4 binding sites were found in the promoter regions of all five genes encoding these DSB repair proteins (Figure 6F). Quantitative chromatin immunoprecipitation (ChIP) analysis indicated that SMAD3 binds to these promoters (Figure 6G), and luciferase-based transactivation assays confirmed that SMAD3 can induce the transactivation of these genes (Figures 6H and 6I). The partial inhibition of the transactivation of some genes (e.g., ATM, DNA-PKcs, and LIG4 by SMAD3i SIS3) (Figure 6I), when compared to the strong downregulation of these genes at the mRNA and protein levels (Figures 6B and 6C, respectively) may be due to experimental limitations and/or indicate SMAD3-dependent post-transcriptional modifications.

Since in the BMM-dc the expression of neither miR-182 nor miR-183 is affected by the CRISPR-Cas9-mediated downregulation of TGFβR2 in the CML-BP K562 cell line and by the SB431542-mediated inhibition of TGFβR kinase signaling in AML primary cells (Figure S6B), we postulate that miR-182 and miR-183 do not play a significant role in the regulation of TGFβR-mediated sensitivity to olaparib in leukemia cells.

DISCUSSION

Preclinical studies and clinical trials indicated that tumor cells acquire PARPi resistance during treatment, which is usually associated with the restoration of HR, the loss of PARP1 expression, and/or the loss of DSB end resection regulation (reviewed in D'Andrea, 2018). Here, we report that HR/D-NHEJ-deficient PARPi-sensitive hematopoietic malignant cells are refractory to PARPi in conditions mimicking the BMM. Hypoxia-induced overexpression of TGFβR1/2 by leukemia cells combined with the production of TGF-β1 by stromal cells resulted in the stimulation of the TGFβR serine/threonine kinase-SMAD2/3 canonical pathway in malignant cells. Targeting of TGFβR kinase and SMAD3 reduced the expression of key genes involved in DNA repair (ATM, BRCA1, BRCA2, DNA-PKcs, LIG4), inhibited HR and D-NHEJ activities and restored the sensitivity of malignant hematopoietic cells to PARPi-mediated synthetic lethality. In summary, we identified an unexpected mechanism of resistance to PARPi, which depends on the TGF-β1-mediated activation of TGFβR kinase intracellular signaling in leukemia cells in BM. It is likely that not only leukemia cells but also solid tumor cells metastatic to BM may be protected from PARPi-mediated synthetic lethality.

We reported before that the TKi-mediated inhibition of OTK activity in PBM induced HR/D-NHEJ deficiency (downregulation of BRCA1, RAD51 and LIG4) and sensitivity of quiescent and proliferating LSCs to PARPi (Maifrede et al., 2018; Nieborowska-Skorska et al., 2017a, 2017b; Sullivan-Reed et al., 2018).

Figure 4. TGFβRi Enhanced Anti-Leukemia Effect of PARPi + TKi

(A) Experimental scheme. Leukemia-bearing mice were treated for 7 consecutive days with TGFβRi (10 mg/kg SB431542), TKi (100 mg/kg imatinib or 1 mg/kg quizartinib) + PARPi (0.165 mg/kg talazoparib), and the combination of TKi + PARPi + TGFβRi.

(B) Results represent mean % of GFP$^+$ cells in peripheral blood leukocytes (PBLs), spleen cells (SPLs), and BM cells (BMC) ± SDs from 4–6 mice/group bearing BCR-ABL1 CML-like disease and FLT3(ITD);*Tet2*$^{-/-}$ AML-like disease following treatment with vehicle (black bars), SB431542 (violet bars), TKi (imatinib for BCR-ABL1 CML-like and quizartinib for FLT3[ITD];*Tet2*$^{-/-}$ AML-like disease) + talazoparib (blue bars) and TKi + talazoparib + SB431542 (orange bars). *$p < 0.05$ when compared to TKi + PARPi.

(C) Survival curves and median survival time (MST) of mice bearing a primary leukemia and treated as indicated (n = 10 mice per group); *$p < 0.001$ versus TKi + PARPi.

(D) Survival curves and MST of secondary transplant mice (n = 6 mice per group); *$p < 0.001$ versus TKi + PARPi.

(E and F) Representative images (200× and 400× magnification) of hematoxylin-stained BM tissues from (E) BCR-ABL1 CML-like mice and (F) FLT3(ITD);*Tet2*$^{-/-}$ AML-like mice treated as indicated; GFP$^+$ cells are stained in brown.

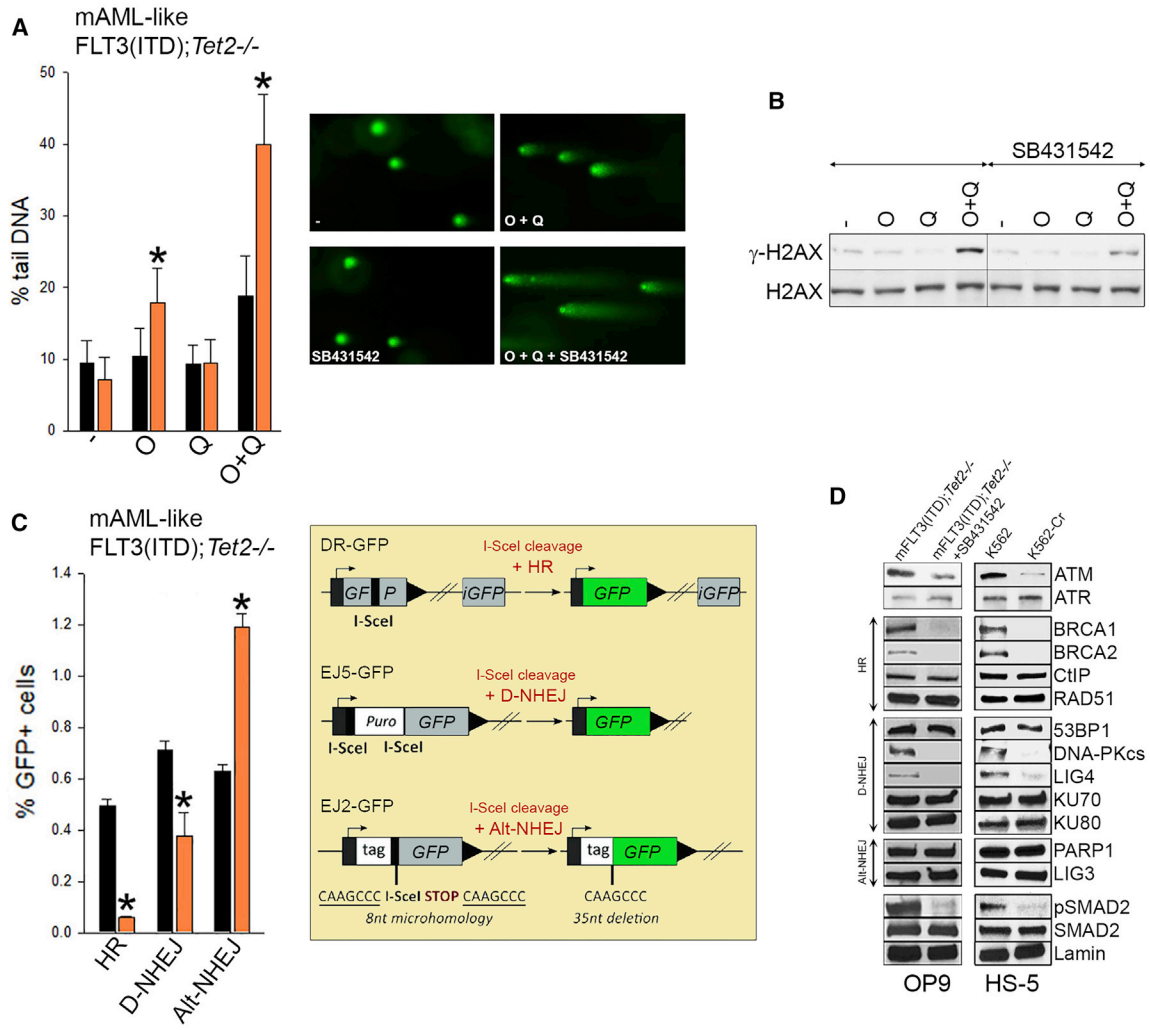

Figure 5. TGFβR Kinase Regulated Accumulation and Repair of DSBs in Leukemia Cells in the BMM

(A) Left panel: murine FLT3(ITD);*Tet2*$^{-/-}$ AML-like cells (3 mice) were treated with diluent (-), 10 μM olaparib (O), 200 nM quizartininb (Q), and the combination (O + Q) in BMM-dc (OP9 stromal cells) in the absence and presence of 10 μM SB431542 (black and orange bars, respectively). The results represent % of tail DNA ± SD in the neutral comet assay. *$p < 0.05$ when compared to the results in BMM-dc. Right panel: representative images of the comets in the indicated conditions.

(B) Western blots showing expression of γ-H2AX and H2AX in nuclear lysates from FLT3(ITD);*Tet2*$^{-/-}$ AML-like cells treated as indicated in (A).

(C) Left panel: HR, D-NHEJ, and Alt-NHEJ repair activities were examined in murine FLT3(ITD);Tet2$^{-/-}$ AML-like cells in BMM-dc in the presence (orange bars) and absence (black bars) of 10 μM SB431542. *$p < 0.05$ when compared to the results in untreated cells. Right panel: scheme of the DSB repair reporter assays. All of the reporter cassettes contain unique *I-SceI* endonuclease restriction sites to induce DSBs triggered by the ectopic expression of I-SceI. The DR-GFP reporter was used to examine HR. *GFP* is a modified *GFP* gene containing *I-SceI* site and in-frame stop codons. An internal *GFP* fragment (*iGFP*) serves as a template for HR repair, resulting in a functional *GFP* gene. The EJ5-GFP reporter was used to examine D-NHEJ. *GFP* is separated from a promoter by a puromycin gene flanked by 2 *I-SceI* sites. The excision of the puromycin gene and D-NHEJ joins the promoter with *GFP,* thus creating a functional *GFP* gene. The EJ2-GFP reporter was used to examine Alt-NHEJ. *GFP* is separated from an N-terminal tag (*NLS/Zinc-finger*) by the *I-SceI* site and stop codon, which are flanked by 8 nt of microhomology. Alt-NHEJ repair results in a functional *GFP* gene by restoring the coding frame between the tag and *GFP*.

(D) Western blots showing the expression of indicated proteins in nuclear lysates from FLT3(ITD);*Tet2*$^{-/-}$ AML-like cells treated or not with 10 μM SB431542, and in K562-wt and TGFβR2-depleted K562-Cr cells in BMM-dc (stromal cells indicated at the bottom).

See also Figure S5.

Since OTK-positive leukemia cells are resistant to TKi in the BMM (Krause and Scadden, 2015), our findings that TGFβRi can mimic the PBM-specific effect of TKi to induce HR/D-NHEJ deficiency in the BMM (downregulation of BRCA1, BRCA2, DNA-PKcs, and LIG4) may have a direct impact on planning therapeutic approaches. Multiple TGFβR kinase inhibitors (galunisertib = LY2157299, TEW-7197, vactosertib, LY3200882) and a TGF-β inhibitor (AVID200) have already entered clinical trials in diverse malignancies; our findings demonstrating the rationale to target TGFβR may lead to prospective therapeutic applications aimed at eliminating HR/D-NHEJ-deficient tumor cells from the BM niche.

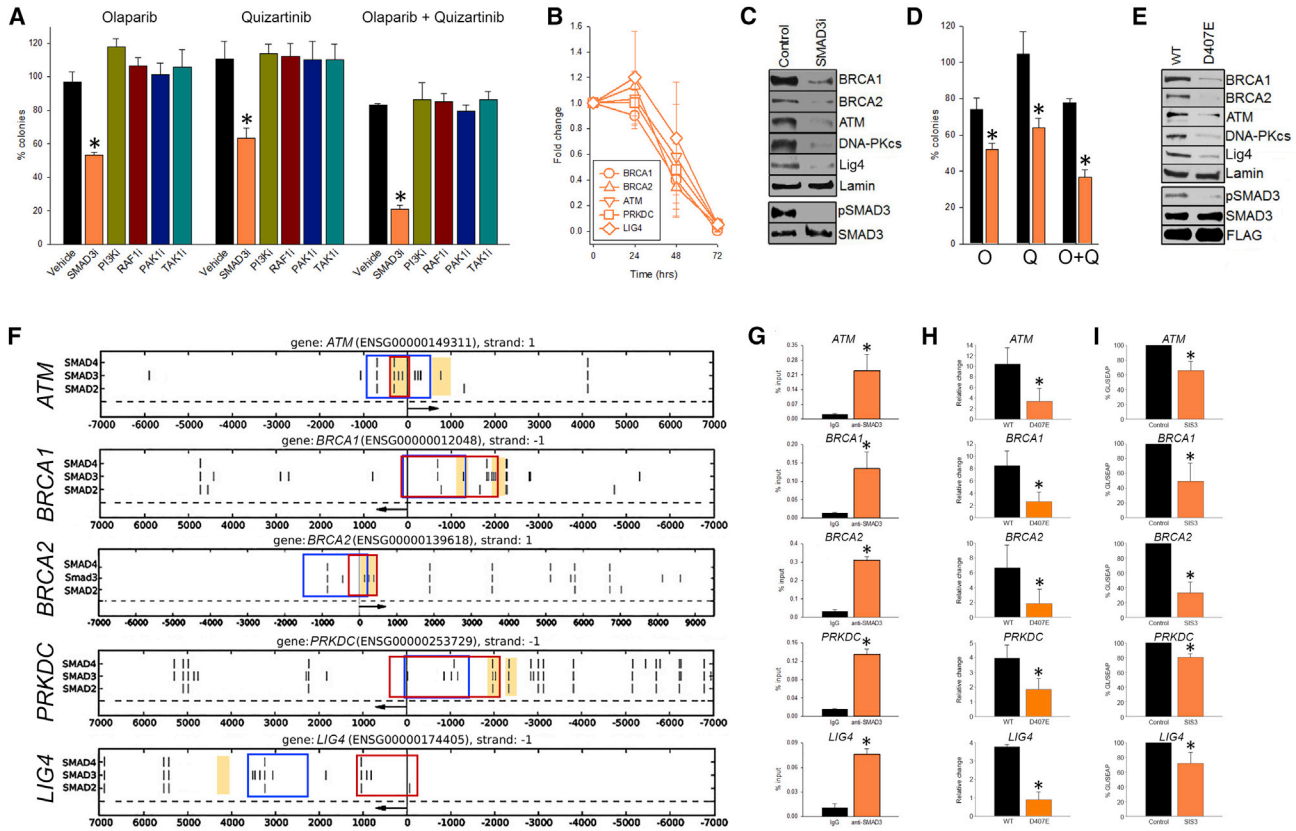

Figure 6. SMAD3 Regulates the Expression of DSB Repair Proteins in the BMM

(A) Murine FLT3(ITD);*Tet2*$^{-/-}$ Lin-cKit^{+} AML-like cells in BMM-dc were left untreated or treated with 1.5 μM olaparib ± 40 nM quizartinib, and 3 μM SMAD3 inhibitor SIS3, 5 μM PI3Ki buparlisib, 2 μM RAF1i LY3009120, 5 μM PAK1i IPA-3, 10 μM TAK1i Takinib, or vehicle for 72 h, followed by plating in methylcellulose. The results represent mean % colonies ± SDs when compared to untreated cells; *p < 0.05 compared to vehicle.

(B) Real-time RT-PCR detecting mRNA levels of the indicated genes in FLT3(ITD) MV-4-11 cells treated with 10 μM SMAD3 inhibitor SIS3 for 24, 48, and 72 h. The results represent the mean ± SD fold change of the mRNA level (2-ΔΔCt) when compared to the vehicle-treated control and normalized to 18SrRNA levels.

(C) Western analysis of the indicated proteins in nuclear lysates from murine FLT3(ITD);*Tet2*$^{-/-}$ cells treated for 72 h with 3 μM SMAD3i SIS3 or vehicle (control).

(D) Clonogenic activity of murine FLT3(ITD);*Tet2*$^{-/-}$ GFP^{+} cells expressing SMAD3(WT) (black bars) or SMAD3(D407E) (orange bars) and treated with 1.5 μM olaparib (O), 40 nM quizartinib (Q), and O + Q. The results represent mean % colonies ± SDs when compared to untreated cells; *p < 0.05 compared to wild type.

(E) Western blot analysis of the indicated DSB repair proteins and pSMAD3, SMAD3, and FLAG-SMAD3(WT) and FLAG-SMAD3(D407E) in nuclear lysates from murine FLT3(ITD);*Tet2*$^{-/-}$ GFP^{+} cells expressing SMAD3(WT) or SMAD3(D407E).

(F) Putative SMAD2/3/4-binding sites in the promoter regions of *ATM*, *BRCA1*, *BRCA2*, *PRKDC* (encodes DNA-PKcs), and *LIG4* detected in the genomic sequences using matrix scan and Markov chain background models. The arrows mark the start of the transcription binding sites. Yellow areas and red and blue boxes: fragments detected or tested in (G), (H) and (I), respectively.

(G) ChIP followed by real-time PCR to detect SMAD3 binding to *ATM*, *BRCA1*, *BRCA2*, *PRKDC*, and *LIG4* promoter regions in AML cells cultured in BMM-dc. The data show mean % DNA input ± SDs; *p < 0.05.

(H) Transactivation activity of the luciferase reporters carrying *ATM*, *BRCA1*, *BRCA2*, *PRKDC*, and *LIG4* promoter regions in 293T cells transfected with SMAD3(WT), SMAD3(D407W), or empty plasmid. The data show the relative change of the promoter region-driven transactivation versus control transfected with empty plasmid ± SD; *p < 0.05.

(I) Transactivation activity of the luciferase reporters carrying *ATM*, *BRCA1*, *BRCA2*, *PRKDC* and *LIG4* promoter regions in MV4-11 cells treated with SIS3 or vehicle (control). The data show % of the promoter-driven Gaussia luciferase (GL)/constitutively expressed secreted alkaline phosphatase (SEAP) activity ± SD; *p < 0.05.

See also Figure S6.

CXCL12-CXCR4 signaling has been often implicated in chemoresistance and TKi resistance of leukemia cells in the BMM (Arrigoni et al., 2018; Karantanou et al., 2018; Zeng et al., 2009). We show that while CXCL12-CXCR4 inhibitors do enhance the sensitivity to TKi in the BMM, they do not affect the sensitivity to PARPi. In striking contrast, the inhibition of the TGFβR kinase-SMAD3 pathway in the BMM sensitized leukemia cells to both TKi and PARPi. Notably, the simultaneous inhibition of CXCR4 and TGFβR did not further enhance the response to PARPi and TKi. Therefore, while our data support the observation that the TGFβR-SMAD3-CXCR4 axis may regulate the sensitivity of leukemia cells to TKi (Nakamura et al., 2015), PARPi resistance appears to be triggered by a different TGFβR-SMAD3-dependent mechanism.

Remarkably, we discovered that the resistance of leukemia cells to PARPi-mediated synthetic lethality in BMM-like conditions depended on the TGFβR kinase-SMAD3 fostered expression of the genes playing a key role in DNA damage recognition (ATM) and in DSB repair by HR (BRCA1, BRCA2) and D-NHEJ (DNA-PKcs, LIG4). ATM-mediated γ-H2AX at DSB sites is required for the initiation of DSB repair (Bonner et al., 2008). HR and D-NHEJ repair DSBs in proliferating cells, D-NHEJ plays a major role in quiescent cells, and Alt-NHEJ serves as backup in both proliferating and quiescent cells (Feng et al., 2011; Karanam et al., 2012). We observed that the inhibition of TGFβR kinase not only reduced the ability to sense DSBs (downregulation of ATM-mediated γ-H2AX) but also altered the capability of DSB repair (downregulation of both HR and D-NHEJ activities and most likely compensatory elevation of Alt-NHEJ). As a result, both proliferating and quiescent leukemia cells became highly sensitive to PARPi in BMM-like conditions. This conclusion is supported by our previous report that PARPi was very effective against HR and D-NHEJ-deficient proliferating and D-NHEJ-deficient quiescent leukemia stem cells in PBM-like conditions (Nieborowska-Skorska et al., 2017b).

There are conflicting reports about the impact of TGF-β1-TGFβR signaling on DSB repair indicating positive and negative effects on the expression of the genes and/or activities of the HR and/or D-NHEJ/Alt-NHEJ pathways (reviewed in Liu et al., 2019). These discrepancies most likely depend on distinct epigenomes (distinct gene expression programs), tumor tissue type (hematologic malignancies, carcinomas, or non-transformed cells), and tumor microenvironment conditions (normoxia versus hypoxia, presence or absence of stromal cells) (Chan et al., 2010; Tufegdzic Vidakovic et al., 2015). We combined hypoxia with the presence of stromal cells in 2- and 3-dimensional co-culture to better mimic *in vitro* BMM-like conditions. Moreover, the critical role of TGFβR kinase signaling in the BMM-dependent resistance of hematologic malignancies to the PARPi ± TKi combination identified by us *in vitro* was validated *in vivo* by demonstrating that the pharmacological inhibitor of TGFβR kinase enhanced the anti-leukemia effect of PARPi + TKi in the BM but not in the PB of SCID mice.

It is worth considering that genetic aberrations may dictate the role of TGF-β1-TGFβR kinase-dependent signaling in the DNA damage response. We postulate that TGFβRi reduces HR and D-NHEJ activity and sensitizes hematopoietic malignancies driven by OTKs such as FLT3(ITD), JAK2(V617F), and BCR-ABL1 to PARPi ± TKi in the BMM. Of note, the mutation-dependent disruption of FANCD2, FANCA, and FANCG (Fanconi anemia [FA] pathway) caused transcriptional changes that resulted in hyperactive TGF-β signaling in hematopoietic stem cells, and the inhibition of the TGF-β pathway in FA cells diminished NHEJ but promoted HR activity (Zhang et al., 2016). Therefore, the anti-leukemia effect of TGFβRi combined with PARPi may be limited in the BM of FA patients.

In conclusion, we discovered an intrinsic mechanism of resistance to PARPi, which depends on the TGF-β1-mediated activation of TGFβR kinase-SMAD2/3 signaling, resulting in the stimulation of DSB repair by HR and D-NHEJ in hematopoietic malignant cells residing in the BM. Although we excluded the CXCL12-CXCR4 axis, additional mechanisms may complement TGF-β1-TGFβR kinase-SMAD2/3 signaling to induce PARPi resistance in BMM.

We postulate that the pharmacological targeting of the TGFβR kinase can improve therapeutic outcomes in leukemic patients receiving PARPis and other drugs, whose activities are limited in the BM niche due to enhanced DSB repair (Zhou et al., 2016). A similar approach may also be applied to treat solid tumors (Liu et al., 2018). In addition, tumors carrying *TGFBR2* deletions/mutations should be responsive to PARPi in the BMM (The ICGC/TCGA Pan-Cancer Analysis of Whole Genomes Consortium, 2020).

STAR★METHODS

Detailed methods are provided in the online version of this paper and include the following:

- KEY RESOURCES TABLE
- RESOURCE AVAILABILITY
  - Lead Contact
  - Materials Availability
  - Data and Code Availability
- EXPERIMENTAL MODEL AND SUBJECT DETAILS
  - *In vitro* studies
  - Animal studies
- METHOD DETAILS
  - BMM and PBM experiments
  - BMM three-dimensional (BMM-3d) co-culture
  - Western blot
  - Downregulation of TGF-β1 in HS-5 cells
  - Retroviral infections
  - DNA damage/repair
  - Immunofluorescence
  - Real-time RT-PCR
  - ChIP
  - Firefly/Renilla Luciferases transactivation assay
  - Gaussia Luciferase/Secreted Alkaline Phosphatase transactivation assay
  - Detection of SMAD2/3/4 putative binding sites
  - MicroRNA quantification
  - Immunohistochemistry
- QUANTIFICATION AND STATISTICAL ANALYSIS

SUPPLEMENTAL INFORMATION

Supplemental Information can be found online at https://doi.org/10.1016/j.celrep.2020.108221.

ACKNOWLEDGMENTS

This work was funded by NIH R01CA186238, R01CA244044, and R01CA247707; the Leukemia and Lymphoma Society Translational Research Program award 6565-19; and the When Everyone Survives Foundation (to T.S.). B.V.L. has been supported by the European Union's Horizon 2020 Research and Innovation Programme under the Marie Sklodowska-Curie grant agreement no. 665735 and by the funding from Polish Ministry of Science and Higher Education funds for the implementation of international projects, 2016–2020 (to K.P.). K.S.-R. was supported by T32CA009009035-43 from NIH. P.P.-B. has been supported by the Hollis Brownstein New Investigator Research Grant from the Leukemia Research Foundation (funding cycle

2018–2019) and research grants from the National Science Centre (2014/15/D/NZ3/05187 and 2018/30/M/NZ3/00274). P.V. was supported by the Austrian Science Fund (FWF) research grants F4701-B28 and F4704-B28. We thank the Laboratory of Animal Models, Nencki Institute of Experimental Biology, Warsaw for the generation of lentivirally transferred MV4-11 cells. This work was supported by the ANIMOD project within the Team Tech Core Facility Plus program of the Foundation for Polish Science, co-financed by the European Union under the European Regional Development Fund.

AUTHOR CONTRIBUTIONS

B.V.L., P.P.-B., S.M., K.S.-R., M.N.-S., K.G., J.-C.Y., R.N., K.Q.C., J.S., M.D., and Z.L. performed the experiments. E.M.P. provided the genetically characterized AML samples from E1900, and R.L.L. performed the somatic sequencing studies of the E1900 samples. H.F.F. led trial E1900, M.S.T. was the ECOG-ACRIN Leukemia Committee chair when E1900 was activated, and M.R.L. is the current ECOG-ACRIN Leukemia Committee chair. P.V. provided the genetically characterized AML samples. G.A.C. and D.L. provided the genetically modified mice. J.H. supervised Z.L. M.A.W. supervised R.N. and K.Q.C. and critically reviewed the manuscript. T.S. and K.P. designed the studies, supervised the experiments, and wrote the manuscript.

DECLARATION OF INTERESTS

The authors declare no competing interests.

Received: April 8, 2020
Revised: August 18, 2020
Accepted: September 10, 2020
Published: October 6, 2020

REFERENCES

Arrigoni, E., Del Re, M., Galimberti, S., Restante, G., Rofi, E., Crucitta, S., Baratè, C., Petrini, M., Danesi, R., and Di Paolo, A. (2018). Concise Review: Chronic Myeloid Leukemia: Stem Cell Niche and Response to Pharmacologic Treatment. Stem Cells Transl. Med. *7*, 305–314.

Barnes, D.J., and Melo, J.V. (2006). Primitive, quiescent and difficult to kill: the role of non-proliferating stem cells in chronic myeloid leukemia. Cell Cycle *5*, 2862–2866.

Bennardo, N., Cheng, A., Huang, N., and Stark, J.M. (2008). Alternative-NHEJ is a mechanistically distinct pathway of mammalian chromosome break repair. PLOS Genet. *4*, e1000110.

Blume-Jensen, P., and Hunter, T. (2001). Oncogenic kinase signalling. Nature *411*, 355–365.

Bolton-Gillespie, E., Schemionek, M., Klein, H.U., Flis, S., Hoser, G., Lange, T., Nieborowska-Skorska, M., Maier, J., Kerstiens, L., Koptyra, M., et al. (2013). Genomic instability may originate from imatinib-refractory chronic myeloid leukemia stem cells. Blood *121*, 4175–4183.

Bonner, W.M., Redon, C.E., Dickey, J.S., Nakamura, A.J., Sedelnikova, O.A., Solier, S., and Pommier, Y. (2008). GammaH2AX and cancer. Nat. Rev. Cancer *8*, 957–967.

Brunen, D., Willems, S.M., Kellner, U., Midgley, R., Simon, I., and Bernards, R. (2013). TGF-β: an emerging player in drug resistance. Cell Cycle *12*, 2960–2968.

Bryant, H.E., Schultz, N., Thomas, H.D., Parker, K.M., Flower, D., Lopez, E., Kyle, S., Meuth, M., Curtin, N.J., and Helleday, T. (2005). Specific killing of BRCA2-deficient tumours with inhibitors of poly(ADP-ribose) polymerase. Nature *434*, 913–917.

Césaire, M., Thariat, J., Candéias, S.M., Stefan, D., Saintigny, Y., and Chevalier, F. (2018). Combining PARP inhibition, radiation, and immunotherapy: a possible strategy to improve the treatment of cancer? Int. J. Mol. Sci. *19*, 3793.

Chan, N., Pires, I.M., Bencokova, Z., Coackley, C., Luoto, K.R., Bhogal, N., Lakshman, M., Gottipati, P., Oliver, F.J., Helleday, T., et al. (2010). Contextual synthetic lethality of cancer cell kill based on the tumor microenvironment. Cancer Res. *70*, 8045–8054.

Chapman, J.R., Taylor, M.R., and Boulton, S.J. (2012). Playing the end game: DNA double-strand break repair pathway choice. Mol. Cell *47*, 497–510.

Chen, E., Ahn, J.S., Massie, C.E., Clynes, D., Godfrey, A.L., Li, J., Park, H.J., Nangalia, J., Silber, Y., Mullally, A., et al. (2014). JAK2V617F promotes replication fork stalling with disease-restricted impairment of the intra-S checkpoint response. Proc. Natl. Acad. Sci. USA *111*, 15190–15195.

Chen, L.L., Lin, H.P., Zhou, W.J., He, C.X., Zhang, Z.Y., Cheng, Z.L., Song, J.B., Liu, P., Chen, X.Y., Xia, Y.K., et al. (2018). SNIP1 Recruits TET2 to Regulate c-MYC Target Genes and Cellular DNA Damage Response. Cell Rep. *25*, 1485–1500.e4.

Cimmino, L., Dolgalev, I., Wang, Y., Yoshimi, A., Martin, G.H., Wang, J., Ng, V., Xia, B., Witkowski, M.T., Mitchell-Flack, M., et al. (2017). Restoration of TET2 Function Blocks Aberrant Self-Renewal and Leukemia Progression. Cell *170*, 1079–1095.e20.

Cramer-Morales, K., Nieborowska-Skorska, M., Scheibner, K., Padget, M., Irvine, D.A., Sliwinski, T., Haas, K., Lee, J., Geng, H., Roy, D., et al. (2013). Personalized synthetic lethality induced by targeting RAD52 in leukemias identified by gene mutation and expression profile. Blood *122*, 1293–1304.

D'Andrea, A.D. (2018). Mechanisms of PARP inhibitor sensitivity and resistance. DNA Repair (Amst.) *71*, 172–176.

Dabrowski, M., Dojer, N., Krystkowiak, I., Kaminska, B., and Wilczynski, B. (2015). Optimally choosing PWM motif databases and sequence scanning approaches based on ChIP-seq data. BMC Bioinformatics *16*, 140.

Dasgupta, Y., Koptyra, M., Hoser, G., Kantekure, K., Roy, D., Gornicka, B., Nieborowska-Skorska, M., Bolton-Gillespie, E., Cerny-Reiterer, S., Müschen, M., et al. (2016). Normal ABL1 is a tumor suppressor and therapeutic target in human and mouse leukemias expressing oncogenic ABL1 kinases. Blood *127*, 2131–2143.

Duan, C.W., Shi, J., Chen, J., Wang, B., Yu, Y.H., Qin, X., Zhou, X.C., Cai, Y.J., Li, Z.Q., Zhang, F., et al. (2014). Leukemia propagating cells rebuild an evolving niche in response to therapy. Cancer Cell *25*, 778–793.

Esposito, M.T., Zhao, L., Fung, T.K., Rane, J.K., Wilson, A., Martin, N., Gil, J., Leung, A.Y., Ashworth, A., and So, C.W. (2015). Synthetic lethal targeting of oncogenic transcription factors in acute leukemia by PARP inhibitors. Nat. Med. *21*, 1481–1490.

Faraoni, I., Giansanti, M., Voso, M.T., Lo-Coco, F., and Graziani, G. (2019). Targeting ADP-ribosylation by PARP inhibitors in acute myeloid leukaemia and related disorders. Biochem. Pharmacol. *167*, 133–148.

Farmer, H., McCabe, N., Lord, C.J., Tutt, A.N., Johnson, D.A., Richardson, T.B., Santarosa, M., Dillon, K.J., Hickson, I., Knights, C., et al. (2005). Targeting the DNA repair defect in BRCA mutant cells as a therapeutic strategy. Nature *434*, 917–921.

Feng, Z., Scott, S.P., Bussen, W., Sharma, G.G., Guo, G., Pandita, T.K., and Powell, S.N. (2011). Rad52 inactivation is synthetically lethal with BRCA2 deficiency. Proc. Natl. Acad. Sci. USA *108*, 686–691.

Georgiades, P., Ogilvy, S., Duval, H., Licence, D.R., Charnock-Jones, D.S., Smith, S.K., and Print, C.G. (2002). VavCre transgenic mice: a tool for mutagenesis in hematopoietic and endothelial lineages. Genesis *34*, 251–256.

Goto, D., Yagi, K., Inoue, H., Iwamoto, I., Kawabata, M., Miyazono, K., and Kato, M. (1998). A single missense mutant of Smad3 inhibits activation of both Smad2 and Smad3, and has a dominant negative effect on TGF-beta signals. FEBS Lett. *430*, 201–204.

Heldin, C.H., and Moustakas, A. (2016). Signaling Receptors for TGF-β Family Members. Cold Spring Harb. Perspect. Biol. *8*, a022053.

Karanam, K., Kafri, R., Loewer, A., and Lahav, G. (2012). Quantitative live cell imaging reveals a gradual shift between DNA repair mechanisms and a maximal use of HR in mid S phase. Mol. Cell *47*, 320–329.

Karantanou, C., Godavarthy, P.S., and Krause, D.S. (2018). Targeting the bone marrow microenvironment in acute leukemia. Leuk. Lymphoma *59*, 2535–2545.

Khorashad, J.S., and Deininger, M.W. (2011). Selection of therapy: rational decisions based on molecular events. Hematol. Oncol. Clin. North Am. *25*, 1009–1023, vi.

Krause, D.S., and Scadden, D.T. (2015). A hostel for the hostile: the bone marrow niche in hematologic neoplasms. Haematologica *100*, 1376–1387.

Krause, D.S., Fulzele, K., Catic, A., Sun, C.C., Dombkowski, D., Hurley, M.P., Lezeau, S., Attar, E., Wu, J.Y., Lin, H.Y., et al. (2013). Differential regulation of myeloid leukemias by the bone marrow microenvironment. Nat. Med. *19*, 1513–1517.

Krystkowiak, I., Lenart, J., Debski, K., Kuterba, P., Petas, M., Kaminska, B., and Dabrowski, M. (2013). Nencki Genomics Database–Ensembl funcgen enhanced with intersections, user data and genome-wide TFBS motifs. Database (Oxford) *2013*, bat069.

Larrosa-Garcia, M., and Baer, M.R. (2017). FLT3 Inhibitors in Acute Myeloid Leukemia: Current Status and Future Directions. Mol. Cancer Ther. *16*, 991–1001.

Lee, B.H., Tothova, Z., Levine, R.L., Anderson, K., Buza-Vidas, N., Cullen, D.E., McDowell, E.P., Adelsperger, J., Fröhling, S., Huntly, B.J., et al. (2007). FLT3 mutations confer enhanced proliferation and survival properties to multipotent progenitors in a murine model of chronic myelomonocytic leukemia. Cancer Cell *12*, 367–380.

Li, L., and Bhatia, R. (2011). Stem cell quiescence. Clin. Cancer Res. *17*, 4936–4941.

Li, Y., Liu, Y., Chiang, Y.J., Huang, F., Li, Y., Li, X., Ning, Y., Zhang, W., Deng, H., and Chen, Y.G. (2019). DNA Damage Activates TGF-β Signaling via ATM-c-Cbl-Mediated Stabilization of the Type II Receptor TβRII. Cell Rep. *28*, 735–745.e4.

Liu, Q., Ma, L., Jones, T., Palomero, L., Pujana, M.A., Martinez-Ruiz, H., Ha, P.K., Murnane, J., Cuartas, I., Seoane, J., et al. (2018). Subjugation of TGFβ Signaling by Human Papilloma Virus in Head and Neck Squamous Cell Carcinoma Shifts DNA Repair from Homologous Recombination to Alternative End Joining. Clin. Cancer Res. *24*, 6001–6014.

Liu, Q., Lopez, K., Murnane, J., Humphrey, T., and Barcellos-Hoff, M.H. (2019). Misrepair in Context: TGFβ Regulation of DNA Repair. Front. Oncol. *9*, 799.

Maifrede, S., Martin, K., Podszywalow-Bartnicka, P., Sullivan-Reed, K., Langer, S.K., Nejati, R., Dasgupta, Y., Hulse, M., Gritsyuk, D., Nieborowska-Skorska, M., et al. (2017). IGH/MYC Translocation Associates with BRCA2 Deficiency and Synthetic Lethality to PARP1 Inhibitors. Mol. Cancer Res. *15*, 967–972.

Maifrede, S., Nieborowska-Skorska, M., Sullivan-Reed, K., Dasgupta, Y., Podszywalow-Bartnicka, P., Le, B.V., Solecka, M., Lian, Z., Belyaeva, E.A., Nersesyan, A., et al. (2018). Tyrosine kinase inhibitor-induced defects in DNA repair sensitize FLT3(ITD)-positive leukemia cells to PARP1 inhibitors. Blood *132*, 67–77.

Marty, C., Lacout, C., Droin, N., Le Couédic, J.P., Ribrag, V., Solary, E., Vainchenker, W., Villeval, J.L., and Plo, I. (2013). A role for reactive oxygen species in JAK2 V617F myeloproliferative neoplasm progression. Leukemia *27*, 2187–2195.

Molenaar, R.J., Radivoyevitch, T., Nagata, Y., Khurshed, M., Przychodzen, B., Makishima, H., Xu, M., Bleeker, F.E., Wilmink, J.W., Carraway, H.E., et al. (2018). *IDH1/2* Mutations Sensitize Acute Myeloid Leukemia to PARP Inhibition and This Is Reversed by IDH1/2-Mutant Inhibitors. Clin. Cancer Res. *24*, 1705–1715.

Moran-Crusio, K., Reavie, L., Shih, A., Abdel-Wahab, O., Ndiaye-Lobry, D., Lobry, C., Figueroa, M.E., Vasanthakumar, A., Patel, J., Zhao, X., et al. (2011). Tet2 loss leads to increased hematopoietic stem cell self-renewal and myeloid transformation. Cancer Cell *20*, 11–24.

Nakamura, T., Shinriki, S., Jono, H., Guo, J., Ueda, M., Hayashi, M., Yamashita, S., Zijlstra, A., Nakayama, H., Hiraki, A., et al. (2015). Intrinsic TGF-β2-triggered SDF-1-CXCR4 signaling axis is crucial for drug resistance and a slow-cycling state in bone marrow-disseminated tumor cells. Oncotarget *6*, 1008–1019.

Nieborowska-Skorska, M., Kopinski, P.K., Ray, R., Hoser, G., Ngaba, D., Flis, S., Cramer, K., Reddy, M.R., Koptyra, M., Penserga, T., et al. (2012). Rac2-MRC-cIII-generated ROS cause genomic instability in chronic myeloid leukemia stem cells and primitive progenitors. Blood *119*, 4253–4263.

Nieborowska-Skorska, M., Maifrede, S., Dasgupta, Y., Sullivan, K., Flis, S., Le, B.V., Solecka, M., Belyaeva, E.A., Kubovcakova, L., Nawrocki, M., et al. (2017a). Ruxolitinib-induced defects in DNA repair cause sensitivity to PARP inhibitors in myeloproliferative neoplasms. Blood *130*, 2848–2859.

Nieborowska-Skorska, M., Sullivan, K., Dasgupta, Y., Podszywalow-Bartnicka, P., Hoser, G., Maifrede, S., Martinez, E., Di Marcantonio, D., Bolton-Gillespie, E., Cramer-Morales, K., et al. (2017b). Gene expression and mutation-guided synthetic lethality eradicates proliferating and quiescent leukemia cells. J. Clin. Invest. *127*, 2392–2406.

Passamonti, F., and Maffioli, M. (2018). The role of JAK2 inhibitors in MPNs 7 years after approval. Blood *131*, 2426–2435.

Patel, J.P., Gönen, M., Figueroa, M.E., Fernandez, H., Sun, Z., Racevskis, J., Van Vlierberghe, P., Dolgalev, I., Thomas, S., Aminova, O., et al. (2012). Prognostic relevance of integrated genetic profiling in acute myeloid leukemia. N. Engl. J. Med. *366*, 1079–1089.

Perrotti, D., Jamieson, C., Goldman, J., and Skorski, T. (2010). Chronic myeloid leukemia: mechanisms of blastic transformation. J. Clin. Invest. *120*, 2254–2264.

Piao, J., Takai, S., Kamiya, T., Inukai, T., Sugita, K., Ohyashiki, K., Delia, D., Masutani, M., Mizutani, S., and Takagi, M. (2017). Poly (ADP-ribose) polymerase inhibitors selectively induce cytotoxicity in TCF3-HLF-positive leukemic cells. Cancer Lett. *386*, 131–140.

Pierce, A.J., Johnson, R.D., Thompson, L.H., and Jasin, M. (1999). XRCC3 promotes homology-directed repair of DNA damage in mammalian cells. Genes Dev. *13*, 2633–2638.

Podszywalow-Bartnicka, P., Wolczyk, M., Kusio-Kobialka, M., Wolanin, K., Skowronek, K., Nieborowska-Skorska, M., Dasgupta, Y., Skorski, T., and Piwocka, K. (2014). Downregulation of BRCA1 protein in BCR-ABL1 leukemia cells depends on stress-triggered TIAR-mediated suppression of translation. Cell Cycle *13*, 3727–3741.

Podszywalow-Bartnicka, P., Maifrede, S., Le, B.V., Nieborowska-Skorska, M., Piwocka, K., and Skorski, T. (2019). PARP1 inhibitor eliminated imatinib-refractory chronic myeloid leukemia cells in bone marrow microenvironment conditions. Leuk. Lymphoma *60*, 262–264.

Roy, R., Chun, J., and Powell, S.N. (2011). BRCA1 and BRCA2: different roles in a common pathway of genome protection. Nat. Rev. Cancer *12*, 68–78.

Sallmyr, A., Fan, J., Datta, K., Kim, K.T., Grosu, D., Shapiro, P., Small, D., and Rassool, F. (2008). Internal tandem duplication of FLT3 (FLT3/ITD) induces increased ROS production, DNA damage, and misrepair: implications for poor prognosis in AML. Blood *111*, 3173–3182.

Scheijen, B., and Griffin, J.D. (2002). Tyrosine kinase oncogenes in normal hematopoiesis and hematological disease. Oncogene *21*, 3314–3333.

Schelker, R.C., Iberl, S., Müller, G., Hart, C., Herr, W., and Grassinger, J. (2018). TGF-β1 and CXCL12 modulate proliferation and chemotherapy sensitivity of acute myeloid leukemia cells co-cultured with multipotent mesenchymal stromal cells. Hematology *23*, 337–345.

Schepers, K., Campbell, T.B., and Passegué, E. (2015). Normal and leukemic stem cell niches: insights and therapeutic opportunities. Cell Stem Cell *16*, 254–267.

Shen, Y., Rehman, F.L., Feng, Y., Boshuizen, J., Bajrami, I., Elliott, R., Wang, B., Lord, C.J., Post, L.E., and Ashworth, A. (2013). BMN 673, a novel and highly potent PARP1/2 inhibitor for the treatment of human cancers with DNA repair deficiency. Clin. Cancer Res. *19*, 5003–5015.

Shi, J., Feng, J., Xie, J., Mei, Z., Shi, T., Wang, S., Du, Y., Yang, G., Wu, Y., Cheng, X., et al. (2017). Targeted blockade of TGF-β and IL-6/JAK2/STAT3 pathways inhibits lung cancer growth promoted by bone marrow-derived myofibroblasts. Sci. Rep. *7*, 8660.

Shimada, A. (2019). Hematological malignancies and molecular targeting therapy. Eur. J. Pharmacol. *862*, 172641.

Stringer, B.W., Day, B.W., D'Souza, R.C.J., Jamieson, P.R., Ensbey, K.S., Bruce, Z.C., Lim, Y.C., Goasdoué, K., Offenhäuser, C., Akgül, S., et al. (2019). A reference collection of patient-derived cell line and xenograft models of proneural, classical and mesenchymal glioblastoma. Sci. Rep. *9*, 4902.

Sullivan-Reed, K., Bolton-Gillespie, E., Dasgupta, Y., Langer, S., Siciliano, M., Nieborowska-Skorska, M., Hanamshet, K., Belyaeva, E.A., Bernhardy, A.J., Lee, J., et al. (2018). Simultaneous Targeting of PARP1 and RAD52 Triggers Dual Synthetic Lethality in BRCA-Deficient Tumor Cells. Cell Rep. *23*, 3127–3136.

Tabe, Y., and Konopleva, M. (2017). Leukemia Stem Cells Microenvironment. Adv. Exp. Med. Biol. *1041*, 19–32.

The ICGC/TCGA Pan-Cancer Analysis of Whole Genomes Consortium (2020). Pan-cancer analysis of whole genomes. Nature *578*, 82–93.

Tobin, L.A., Robert, C., Rapoport, A.P., Gojo, I., Baer, M.R., Tomkinson, A.E., and Rassool, F.V. (2013). Targeting abnormal DNA double-strand break repair in tyrosine kinase inhibitor-resistant chronic myeloid leukemias. Oncogene *32*, 1784–1793.

Tufegdzic Vidakovic, A., Rueda, O.M., Vervoort, S.J., Sati Batra, A., Goldgraben, M.A., Uribe-Lewis, S., Greenwood, W., Coffer, P.J., Bruna, A., and Caldas, C. (2015). Context-Specific Effects of TGF-β/SMAD3 in Cancer Are Modulated by the Epigenome. Cell Rep. *13*, 2480–2490.

Turatsinze, J.V., Thomas-Chollier, M., Defrance, M., and van Helden, J. (2008). Using RSAT to scan genome sequences for transcription factor binding sites and cis-regulatory modules. Nat. Protoc. *3*, 1578–1588.

Vander Ark, A., Cao, J., and Li, X. (2018). TGF-β receptors: in and beyond TGF-β signaling. Cell. Signal. *52*, 112–120.

Yap, T.A., Sandhu, S.K., Carden, C.P., and de Bono, J.S. (2011). Poly(ADP-ribose) polymerase (PARP) inhibitors: exploiting a synthetic lethal strategy in the clinic. CA Cancer J. Clin. *61*, 31–49.

Zeng, Z., Shi, Y.X., Samudio, I.J., Wang, R.Y., Ling, X., Frolova, O., Levis, M., Rubin, J.B., Negrin, R.R., Estey, E.H., et al. (2009). Targeting the leukemia microenvironment by CXCR4 inhibition overcomes resistance to kinase inhibitors and chemotherapy in AML. Blood *113*, 6215–6224.

Zhang, H., Kozono, D.E., O'Connor, K.W., Vidal-Cardenas, S., Rousseau, A., Hamilton, A., Moreau, L., Gaudiano, E.F., Greenberger, J., Bagby, G., et al. (2016). TGF-β Inhibition Rescues Hematopoietic Stem Cell Defects and Bone Marrow Failure in Fanconi Anemia. Cell Stem Cell *18*, 668–681.

Zhou, H.S., Carter, B.Z., and Andreeff, M. (2016). Bone marrow niche-mediated survival of leukemia stem cells in acute myeloid leukemia: Yin and Yang. Cancer Biol. Med. *13*, 248–259.

Zhou, J., Zhang, C., Zhou, B., and Jiang, D. (2019). miR-183 modulated cell proliferation and apoptosis in ovarian cancer through the TGF-β/Smad4 signaling pathway. Int. J. Mol. Med. *43*, 1734–1746.

STAR★METHODS

KEY RESOURCES TABLE

REAGENT or RESOURCE	SOURCE	IDENTIFIER
Antibodies		
TGFβR2	Invitrogen	Cat# 701683; RRID:AB_2608868
TGFβR1	Santa Cruz Biotechnology	Cat# sc-518018
Phospho-SMAD2	Cell Signaling Technology	Cat# 3108; RRID:AB_490941
SMAD2	Cell Signaling Technology	Cat# 5339; RRID:AB_10626777
Phospho-SMAD3	Cell Signaling Technology	Cat# 9520; RRID:AB_2193207
SMAD3	Cell Signaling Technology	Cat# 9523; RRID:AB_2193182
Phospho-AKT	Cell Signaling Technology	Cat# 9271; RRID:AB_329825
AKT	Cell Signaling Technology	Cat# 2920; RRID:AB_1147620
Phospho-ERK1/2	Cell Signaling Technology	Cat# 4370; RRID:AB_2315112
ERK1/2	Cell Signaling Technology	Cat# 4696; RRID:AB_390780
Phospho-p38/MAPK	Cell Signaling Technology	Cat# 9216; RRID:AB_331296
p38/MAPK	Invitrogen	Cat# 33-1300; RRID:AB_2533100
BRCA1	Millipore	Cat# OP92; RRID:AB_2750876
BRCA2	Abcam	Cat# ab75335; RRID:AB_2067758
ATM	Santa Cruz Biotechnology	Cat# sc-135663; RRID:AB_2062962
Phospho-Histone H2AX (γ-H2AX)	Cell Signaling Technology	Cat# 9718; RRID:AB_2118009
Histone H2AX	Cell Signaling Technology	Cat# 2595; RRID:AB_10694556
Phospho-ATM	Santa Cruz Biotechnology	Cat# sc-47739; RRID:AB_781524
ATR	Santa Cruz Biotechnology	Cat# sc-515173
DNA-PKcs	Bethyl	Cat# A300-518A; RRID:AB_451043
DNA Ligase IV	Santa Cruz Biotechnology	Cat# sc-271299; RRID:AB_10610371
RAD51	Santa Cruz Biotechnology	Cat# sc-8349; RRID:AB_2253533
Ku80	Invitrogen	Cat# MA5-15873; RRID:AB_11156182
Ku70	Santa Cruz Biotechnology	Cat# sc-17789; RRID:AB_628454
53BP1	Abcam	Cat# ab-21083; RRID:AB_722496
CtIP	Invitrogen	Cat# PA5-20963; RRID:AB_11153016
PARP1	Santa Cruz Biotechnology	Cat# sc-74470; RRID:AB_1127036
DNA Ligase III	Santa Cruz Biotechnology	Cat# sc-135883; RRID:AB_2136237
DNA Polymerase θ	Invitrogen	Cat# PA5-69577; RRID:AB_2688722
Lamin	Abcam	Cat# ab-16048; RRID:AB_10107828
β-actin	Santa Cruz Biotechnology	Cat# sc-47778; RRID:AB_2714189
FLAG	Cell Signaling Technology	Cat# 2368S; RRID:AB_2217020
Phosphotyrosine 4G10	Millipore	Cat# 16-205; RRID:AB_310802
HRP-conjugated rabbit IgG	Millipore	Cat# 12-348; RRID:AB_390191
HRP-conjugated mouse IgG	Millipore	Cat# 12-349; RRID:AB_390192
Rabbit IgG, Alexa 488	Invitrogen	Cat# A-11034; RRID:AB_2576217
Mouse IgG, Alexa 488	Invitrogen	Cat# A-11001; RRID:AB_2534069
TGFβ-1,2,3 neutralizing antibody 1D11.16.8	Invitrogen	Cat# 16-9243-85; RRID:AB_2573124
Linage antibody cocktail	BD Biosciences	Cat# 340546; RRID:AB_400053
CD34	BD Biosciences	Cat# 347203; RRID:AB_400266
CD38	BD Biosciences	Cat# 555460; RRID:AB_395853
GFP	Invitrogen	Cat# 11122; RRID:AB_221569

(*Continued on next page*)

Continued

REAGENT or RESOURCE	SOURCE	IDENTIFIER
Biological Samples		
Murine femoral bone marrow tissue specimens	This paper	N/A
Murine tail vein peripheral blood	This paper	N/A
Murine spleen specimens	This paper	N/A
Chemicals, Peptides, and Recombinant Proteins		
SB435142 (TGFβR inhibitor)	Selleckchem	Cat# S1067
Galunisertib (TGFβR inhibitor)	Selleckchem	Cat# S2230
AMD3100 (CXCR4i antagonist)	Selleckchem	Cat# S8030
WZ811(CXCR4i antagonist)	Selleckchem	Cat# S2912
Olaparib (PARP inhibitor)	Selleckchem	Cat# S1060
Talazoparib (PARP inhibitor)	Selleckchem	Cat# S7048
Quizartinib (FLT3 inhibitor)	Selleckchem	Cat# S1526
Imatinib (ABL inhibitor)	Selleckchem	Cat# S2475
SIS3 (SMAD3 inhibitor)	Selleckchem	Cat# S7959
Buparlisib (PI3K inhibitor)	Selleckchem	Cat# S2247
LY3009120 (RAF inhibitor)	Selleckchem	Cat# S7842
IPA-3 (PAK1 inhibitor)	Selleckchem	Cat# S7093
Takinib (TAK1 inhibitor)	Selleckchem	Cat# S8663
4-hydroxytamoxifen	Sigma Aldrich	Cat# H7904
TGF-β1 (human)	Invitrogen	Cat# PHG9204
TGF-β1 (mouse)	R&D Systems	Cat# 7666-MB-005
SCF (human)	StemCell Technologies	Cat# 78155.2
SCF (mouse)	StemCell Technologies	Cat# 78064.2
FLT3	Stem Cell Technologies	Cat# 78137.2
IL-3 (human)	StemCell Technologies	Cat# 78040.2
IL-3 (mouse)	PeproTech	Cat# 213-13
IL-6	StemCell Technologies	Cat# 78050.2
G-CSF	StemCell Technologies	Cat# 78012.2
TPO	PeproTech	Cat# 300-18
Cell Proliferation Dye eFluor 670	Invitrogen	Cat# 65-0840
RIPA buffer	Thermo Fisher Scientific	Cat# 89900
Pierce ECL Western Blotting Substrate	Thermo Fisher Scientific	Cat# 32106
I-SceI	Thermo Fisher Scientific	Cat# ER1771
XhoI	Promega	Cat# R6161
KpnI	Promega	Cat# R6341
MesenCult™ MSC Basal Medium (Human)	StemCell Technologies	Cat# 05401
MesenCult MSC Stimulatory Supplement (Human)	StemCell Technologies	Cat# 05402
FC receptor block solution	Biolegend	Cat# 422302
StemSpan™ SFEM II	StemCell Technologies	Cat# 09655
MethoCult H4230	StemCell Technologies	Cat# 04230
TRI Reagent	Sigma Aldrich	Cat# T9424
M-MLV enzyme	Promega	Cat# M1705
Oligo dT	Bioline	Cat# BIO-38029
Random hexamers	Bioline	Cat# BIO-38028
RNase inhibitor	Blirt	Cat# RT36
SensiFAST SYBR Green Hi-ROX	Bioline	Cat# BIO-92020

(*Continued on next page*)

Continued

REAGENT or RESOURCE	SOURCE	IDENTIFIER
Q5 High-Fidelity DNA polymerase	New England Biolabs	Cat# M0491
Lipofectamine 2000	Invitrogen	Cat# 11668019
Cell line Nucleofector kit V	Lonza	Cat# VCA-1003
Polybrene	Sigma	Cat# TR-1003
Critical Commercial Assays		
OxiSelect Comet Assay Kit	Cell Biolabs	Cat# STA-351
EasySep mouse hematopoietic progenitor cell isolation kit	StemCell Technologies	Cat# 19856
EasySep mouse CD117 (KIT) positive selection kit	StemCell Technologies	Cat# 18757
EasySep human hematopoietic progenitor cell enrichment kit	StemCell Technologies	Cat# 14056
EasySep human hematopoietic CD34 positive selection kit	StemCell Technologies	Cat# 17856
4-20% Mini-PROTEAN TGX Precast Protein Gels	BioRad	Cat# 4561094
Nitrocellulose membrane	Thermo Fisher Scientific	Cat# 88018
Human/Mouse TGF-β1 ELISA Ready-SET-Go! Kit	eBioscience	Cat# 88-8350
miRNeasy Micro Kit	QIAGEN	Cat# 217084
Cell Line Nucleofector kit V	Lonza	Cat# VCA-1003
Secrete-Pair Dual Luminescence Assay Kit	GeneCopoeia	Cat# LF031
Dual-Glo Luciferase assay System	Promega	Cat# E2920
Total RNA Mini columns	A&A Biotechnology	Cat# 031-100
0.45-μM PES filter	Millipore	Cat# SLHP033RS
PerFix EXPOSE kit	Beckman Coulter	Cat# B26976
Experimental Models: Cell Lines		
HS-5	ATCC	Cat# CRL-11882; RRID:CVCL_3720
HS-5-TGFβ1 CRISPR/Cas9 knock-down	This paper	N/A
OP-9	ATCC	Cat# CRL-2749; RRID:CVCL_4398
K562	ATCC	Cat# CCL-243; RRID:CVCL_0004
K562-TGFβR2 CRISPR/Cas9 knock-down	Applied Biological Materials Inc.	Cat# NM_003242
Kasumi-1	ATCC	Cat# CRL-2724; RRID:CVCL_0589
MV4-11	ATCC	Cat# CRL-9591; RRID:CVCL_0064
HEK293T/17	ATCC	Cat# CRL-11268; RRID:CVCL_1926
Experimental Models: Organisms/Strains		
NOD.Cg-Prkdc^{scid}/J mice	Jackson Laboratory	Cat# 001303; RRID:IMSR_JAX:001303
B6.Cg-Ndor1$^{Tg(UBC-cre/ERT2)1Ejb}$/1J mice	Jackson Laboratory	Cat# 007001; RRID:IMSR_JAX:007001
B6N.129S6(SJL)-Jak2$^{tm1.2Ble}$/AmlyJ mice	Jackson Laboratory	Cat# 031658; RRID:IMSR_JAX:031658
B6;129-Tgfbr2^{tm1Karl}/J	Jackson Laboratory	Cat# 012603; RRID:IMSR_JAX:012603
Vav-cre mice	Jackson Laboratory	Cat# 018968; RRID:IMSR_JAX:018968
Human AML cells	https://www.nejm.org/doi/full/10.1056/NEJMoa1112304	N/A
Human CML and AML cells	https://www.jci.org/articles/view/90825	N/A
Human MPN cells	https://ashpublications.org/blood/article/130/26/2848/36601/Ruxolitinib-induced-defects-in-DNA-repair-cause	N/A
Human normal bone marrow (CD34$^+$) cells	StemCell Technologies	https://www.stemcell.com/human-bone-marrow-cd34-cells-frozen.html

(*Continued on next page*)

Continued

REAGENT or RESOURCE	SOURCE	IDENTIFIER
Human primary bone marrow mesenchymal stromal cells	StemCell Technologies	Cat #70022
Oligonucleotides		
Forward primer for JAK2(V617F) genotype: CGT GCA TAG TGT CTG TGG AAG TC	This paper	N/A
Reverse primer for JAK2(V617F) genotype: CGT GGA GAG TCT GTA AGG CTC AA	This paper	N/A
Forward primer for UBC-Cre: GCA TTA CCG GTC GAT GCA ACG AGT GAT GAG	This paper	N/A
Reverse primer for UBC-Cre: GAG TGA ACG AAC CTG GTC GAA ATC AGT GCG	This paper	N/A
Forward primer for TGFβR2$^{fl/fl}$ genotype: TAA ACA AGG TCC GGA GCC CA	This paper	N/A
Reverse primer for TGFβR2$^{fl/fl}$ genotype: ACT TCT GCA AGA GGT CCC CT	This paper	N/A
Primers for ChIP – real-time PCR: See Table S2	This paper	N/A
Primers for real-time RT-PCR: See Table S1	This paper	N/A
Primers for generation of transactivation reporters: See Table S3	This paper	N/A
Recombinant DNA		
pcDNA3;FLAG;SMAD3(WT)	https://febs.onlinelibrary.wiley.com/doi/full/10.1016/S0014-5793%2898%2900658-9?sid=nlm%3Apubmed	N/A
pcDNA3;FLAG;SMAD3(D407E)	https://febs.onlinelibrary.wiley.com/doi/full/10.1016/S0014-5793%2898%2900658-9?sid=nlm%3Apubmed	N/A
pMIG-IRES-GFP	pMIG was a gift from William Hahn (http://www.addgene.org/9044/)	Addgene plasmid# 9044; RRID:Addgene_9044
DR-GFP	http://genesdev.cshlp.org/content/13/20/2633.long	Addgene plasmid# 26475; RRID:Addgene_26475
EJ5-GFP	https://journals.plos.org/plosgenetics/article?id=10.1371/journal.pgen.1000110	Addgene plasmid# 44026; RRID:Addgene_44026
EJ2-GFP	https://journals.plos.org/plosgenetics/article?id=10.1371/journal.pgen.1000110	Addgene plasmid# 44025; RRID:Addgene_44025
lentiCRISPRv2	https://idp.nature.com/authorize?response_type=cookie&client_id=grover&redirect_uri=https%3A%2F%2Fwww.nature.com%2Farticles%2Fs41598-019-41277-z	Addgene plasmid# 98290; RRID:Addgene_98290
pLenti7.3-redluc	Invitrogen	Cat #V53406
pCL-ECO	https://jvi.asm.org/content/70/8/5701.long	Addgene Cat# 12371
BRCA1: pEZX-PG04.1	GeneCopoeia	Cat# HPRM47192-PG04
BRCA2: pEZX-PG04.1	GeneCopoeia	Cat# HPRM30044-PG04
ATM: pEZX-PG04.1	GeneCopoeia	Cat# HPRM30037-PG04
Lig4: pEZX-PG04.1	GeneCopoeia	Cat# HPRM44240-PG04
PRKDC: pEZX-PG04.1	GeneCopoeia	Cat# HPRM33722-PG04
pGL3-Basic	Promega	Cat# E1751
pGL4.73	Promega	Cat# E6911

(*Continued on next page*)

Continued

REAGENT or RESOURCE	SOURCE	IDENTIFIER
Software and Algorithms		
ImageJ	OpenComet	https://imagej.nih.gov/ij/
SigmaPlot	Systat software	https://systatsoftware.com/products/sigmaplot/
FlowJo	BD Biosciences	https://www.flowjo.com/solutions/flowjo
Excel	Microsoft	https://www.microsoft.com/en-us/microsoft-365/excel
Command line version of the program matrix-scan (quick)	https://idp.nature.com/authorize?response_type=cookie&client_id=grover&redirect_uri=https%3A%2F%2Fwww.nature.com%2Farticles%2Fnprot.2008.97	http://rsat.sb-roscoff.fr/matrix-scan-quick_form.cgi
Background model: 2nt_upstream-noorf_Homo_sapiens_EnsEMBL-ovlp-2str	https://idp.nature.com/authorize?response_type=cookie&client_id=grover&redirect_uri=https%3A%2F%2Fwww.nature.com%2Farticles%2Fnprot.2008.97	http://pedagogix-tagc.univ-mrs.fr/rsat/download-request_form.cgi
Command line version of the program matrix-distrib	https://idp.nature.com/authorize?response_type=cookie&client_id=grover&redirect_uri=https%3A%2F%2Fwww.nature.com%2Farticles%2Fnprot.2008.97	http://rsat.sb-roscoff.fr/matrix-distrib_form.cgi
Web service function PlotGenomic	https://academic.oup.com/database/article/doi/10.1093/database/bat069/342206	http://webservices.nencki-genomics.org:8080/genomic?wsdl should be accessed using one of the WSDL client programs, available for download on the wiki page of the Nencki Genomics Database http://www.nencki-genomics.org/wiki/doku.php?id=tutorial:webservices

RESOURCE AVAILABILITY

Lead Contact

Any further inquiries, questions, requests about methodological resources, reagents or experimental procedures can be directly addressed to and will be clarified by the Lead Contact, Tomasz Skorski (tskorski@temple.edu).

Materials Availability

This study did not produce new reagents, chemicals or plasmids.

Data and Code Availability

This study did not generate any datasets or codes.

EXPERIMENTAL MODEL AND SUBJECT DETAILS

In vitro studies

Human malignant and normal hematopoietic cells

FLT3(ITD);*TET2mut*, FLT3(ITD);AML1-ETO and AML1-ETO –positive primary AML samples were from the ECOG-ACRIN E1900 clinical trial (Patel et al., 2012). JAK2(V617F);*TET2mut* and BRCA1/2-deficient AML samples were described before (Nieborowska-Skorska et al., 2017a, 2017b). BCR-ABL1 –positive CML-CP samples were obtained from the Medical University of Vienna and Ludwig-Boltzmann Institute for Hematology and Oncology, Vienna, Austria. Samples of normal hematopoietic cells were purchased from StemCell Technologies (Vancouver, Canada). $Lin^{-}CD34^{+}$ cells were obtained from mononuclear fractions by magnetic sorting using the EasySep Lin negative selection cocktail followed by CD34 positive selection (StemCell Technologies) as described before (Nieborowska-Skorska et al., 2017b). CML-BP K562 cells, AML MV4-11 cells and Kasumi-1 cells were from ATCC. TGFβR2 CRISPR/Cas9 knock-down K562-Cr cells were from Applied Biological Materials Inc. (Vancouver, Canada). These leukemic cell lines were maintained in DMEM supplemented with 10% FBS, L-glutamine and antibiotics in 37°C.

Murine malignant hematopoietic cells

Tet2$^{fl/fl}$ (Moran-Crusio et al., 2011) and *Parp1*−/− (Nieborowska-Skorska et al., 2017b) mice were crossed to FLT3(ITD) (Lee et al., 2007) and Vav-CRE (Georgiades et al., 2002) strains to generate FLT3(ITD);*Tet2*−/− and FLT3(ITD);*Tet2*−/−;*Parp1*−/− mice. *UBC-*^{CreERT2} (B6.Cg-Ndor1$^{Tg(UBC-cre/ERT2)1Ejb}$/1J), *JAK2*$^{V617F/+}$ (B6N.129S6(SJL)-Jak2$^{tm1.2Ble}$/AmlyJ) and *Tgfβr2*$^{f/f}$ (B6;129-Tgfbr2^{tm1Karl}/J) mice (Jackson Laboratories) were crossed to generate *UBC-Cre*^{ERT2};*JAK2*$^{V617F/+}$;*Tgfβr2*$^{f/f}$ and *UBC-Cre*^{ERT2};*JAK2*$^{V617F/+}$;*Tgfβr2*$^{+/+}$ mice. The primers used for mice genotyping are listed in Table S1. The Institutional Animal Care and Use Committee at Washington University approved all animal procedures. JAK2(V617F);*Tgfβr2*−/− and JAK2(V617F);*Tgfβr2*+/+ bone marrow cells were obtained after activation of Cre recombinase during 7 days incubation with 1 μM 4-hydroxytamoxifen (Sigma Aldrich). Expression of JAK2(V617F) and depletion of Tgfβr2 was confirmed by immunofluorescence. Lin$^-$cKit$^+$ cells were obtained from mononuclear fractions by magnetic sorting using the EasySep Lin negative selection followed by cKit positive selection cocktail (StemCell Technologies) as described before (Nieborowska-Skorska et al., 2017b).

Bone marrow (BM) stromal cells

Monolayers of human BM mesenchymal stromal cells (StemCell Technologies) were maintained in MesenCult^{TM} Proliferation kit supplemented with mesenchymal stem cell stimulatory supplements (StemCell Technologies). Primary autologous stroma cells monolayers were established as described by Schelker et al. (Schelker et al., 2018) with modifications. Briefly, a leukemic mouse BM cells and AML patient's BM cells were cultivated for 7-10 days in 48-well plate in DMEM supplemented with 10% FBS, L-glutamine and antibiotics to establish stroma cells monolayer. HS-5 and OP9 cells (ATCC) were cultured in DMEM supplemented with 10% FBS, L-glutamine and antibiotics.

Animal studies

Twelve weeks-old NOD.Cg-Prkdc^{scid}/J (SCID) female mice were purchased from The Jackson Laboratory. SCID mice bearing GFP+ BCR-ABL1 CML-like or GFP+ FLT3(ITD);Tet2−/− AML-like murine leukemias (10%–20% GFP+ leukemia cells in total tail vein blood leukocytes) were treated for 7 consecutive days with vehicle, TKi (100 mg/kg imatinib or 1 mg/kg quizartinib) + PARPi (0.165 mg/kg talazoparib) as described before (Maifrede et al., 2018; Nieborowska-Skorska et al., 2017b), TGFβRi (10 mg/kg SB431542) (Shi et al., 2017) and the combination of TKi + PARPi + TGFβRi (Selleckchem). GFP+ leukemia cells were detected by flow cytometry in peripheral blood leukocytes (PBL), splenocytes (SPL) and bone marrow cells (BMC) 3 days after the end of treatment. Moreover, 1 × 10^6 femoral bone marrow cells were transplanted into the sub-lethally irradiated secondary recipients to assess the effect of treatment on LSCs. Median survival time (MST) of the primary and secondary recipients was determined by Kaplan-Meier survival analysis. The Institutional Animal Care and Use Committee at Temple University approved all animal procedures and the experimental mice were maintained under a completely pathology-free condition and standard feeding diet in the animal facility of Temple University.

METHOD DETAILS

BMM and PBM experiments

To mimic BMM, normal and malignant hematopoietic cells were co-cultured in direct contact (BMM-dc) with stromal cell monolayers (1:1 ratio) in serum-free medium StemSpan^{TM} SFEM II (StemCell Technologies) supplemented with recombinant growth factors, including 100 ng/mL SCF, 100 ng/mL FLT3, 20 ng/mL IL-3, 20 ng/mL IL-6, 20 ng/mL G-CSF and 100 ng/mL TPO as described before (Maifrede et al., 2018; Nieborowska-Skorska et al., 2017a; Nieborowska-Skorska et al., 2017b) in hypoxia (1% O_2) in 37°C. BMM indirect contact (BMM-idc) condition was achieved by separation of stroma and hematopoietic cells with a 0.4 μm PET cell culture insert (Millipore). BMM-cm was achieved by maintaining leukemia cells in 24 hours-conditioned medium from HS-5 cells in hypoxia. PBM condition was mimicked by maintaining malignant and normal hematopoietic cells in liquid culture in normoxia (17% O_2) in the absence of stroma. After 24 hours, inhibitors (listed in the Key Resources Table) were added for 3-5 days followed by evaluation of normal and malignant cells clonogenic activity in MethoCult H4230 (StemCell Technologies), number of Lin$^-$CD34$^+$CD38$^-$CFSE^{max} quiescent cells [flow cytometry using Cell Proliferation Dye eFluor 670 (Invitrogen), Linage cocktail, CD34 and CD38 antibodies (BD Biosciences)], and cell cycle (propidium iodide staining) as described before (Maifrede et al., 2018; Nieborowska-Skorska et al., 2017a; Nieborowska-Skorska et al., 2017b; Podszywalow-Bartnicka et al., 2019).

BMM three-dimensional (BMM-3d) co-culture

MV4-11 cells were lentivirally transfected with plasmid pLenti7.3-redluc expressing GFP and Firefly luciferase (Invitrogen), followed by sorting of GFP+ cells. Co-culture in spheres was achieved by seeding 1000 of MV4-11 cells with 2000 of HS-5 cells in 5% Matrigel^{TM} (Corning) in IMDM medium supplemented with L-glutamine, in a non-adhesive 96 well U-bottom plates (BD Falcon). Seven days later cells were treated for 72h in hypoxia as indicated. Luciferase was assayed using luciferase kit (Promega) and luminescence was measured using Promega Glomax 20/20 luminometer. Protein level in the cell lysates was measured using Bradford solution.

Western blot

Nuclear and total cell lysates were obtained by nuclear lysis buffer and RIPA buffer (Thermo Fisher Scientific) as described before (Cramer-Morales et al., 2013) and analyzed by immunoblotting with primary antibodies listed in the Key Resources Table. In the

procedure, proteins in cell lysates were separated by SDS-PAGE in gradient (4%–20%) Mini-PROTEAN TGX Precast Protein Gels (BioRad). The gels were then transferred into nitrocellulose membranes (Thermo Fisher Scientific) at 4°C by 105 voltage in one hour. To conduct immunoblotting analysis, the membranes were blocked with 5% fat-free milk/BSA solution in one hour at room temperature and primary antibodies were added at desired concentration and incubated overnight at 4°C with gentle shaking. The following day, the membranes were washed thoroughly and given in solution of HRP-conjugated rabbit/mouse anti-IgG antibodies (Millipore) in one hour at room temperature. Protein blots were detected in Premium X-Ray Film (Phenix) by Pierce ECL Western Blotting Substrate (Thermo Fisher Scientific). Lamin and β-actin were used as the loading controls for nuclear and total cell lysates, respectively.

Downregulation of TGF-β1 in HS-5 cells

TGF-β1 in HS-5 cells was downregulated by CRISPR/Cas9. Briefly, guide RNAs (gRNAs) targeting TGF-β1 were generated using CRISPR Design and cloned into the lentiCRISPRv2 vector. The lentiCRISPRv2 vector (Stringer et al., 2019) with a gRNA insert, the packaging plasmid psPAX2, and the envelope plasmid VSVG were mixed together and packed in HEK293T cells using Fugene 6. Lentiviruses were harvested at 48 and 72 h respectively. Then, HS-5 cells were infected at 50% confluency with freshly collected CRISPR-Cas9-gRNA lentivirus supplemented with 8 μg/ml polybrene for 48h. Infected cells were selected in media with puromycin (1 μg/ml) for up to 14 days. Successful mutation of infected HS-5 cell lines was confirmed with T7E1 assay. Secretion of TGF-β1 was tested in supernatants of cell lines cultured in serum free conditions (to avoid background detection of bovine serum TGF-β) by ELISA method using Human/Mouse TGF-β1 ELISA Ready-SET-Go! Kit (eBioscience). Prior to ELISA, cell culture supernatants were first acidified to enable detection also of latent TGF-β1. In brief, 96-well Nunc MaxiSorp plates (Invitrogen, Carlsbad) were first coated with capture antibody overnight and then supernatants were incubated in wells for 2h at RT. Afterward, biotinylated detection antibody and streptavidin-HRP were added to detect the amount of TGF-β1 by enzymatic colorimetric reaction. Absorbance was measured at 450nm using Tecan Sunrise spectrophotometer and X-fluor software. Final concentrations of TGF-β1 in cell culture supernatants were calculated based on the standard curve equation.

Retroviral infections

Dominant-negative murine SMAD3(D407E) mutant and SMAD3 wild-type (WT) cDNAs were obtained from Dr. Mitsuyasu Kato (Goto et al., 1998) and were re-cloned to pMIG-IRES-GFP retroviral construct. Retroviruses were prepared by co-transfecting HEK293T/17 cells (ATCC® CRL-11268) in a 10-cm plate with 10 μg of packaging pCL-ECO plasmid (Addgene #12371) and 10 μg MIGR1 based vectors by using Lipofectamine 2000 transfection reagent (Invirtogen) according to manufacturer's protocol. Viruses were harvested 40h and 64h after the transfection and filtered through a 0.45-μm PES filter (Millipore). For infection, 5×10^5 cells were suspended in 1 mL of virus-containing medium containing 6 μg/ml polybrene (Sigma) and supplemented with recombinant growth factors, including 100 ng/mL SCF, 100 ng/mL FLT3, 20 ng/mL IL-3, and 20 ng/mL IL-6. GFP+ cells were obtained by fluorescent cell sorting 48 hr after the initial infection as described before (Dasgupta et al., 2016).

DNA damage/repair

Neutral comet assay was performed by cell-agarose electrophoresis in Tris-Acetic acid-EDTA buffer based on OxiSelect Comet Assay Kit (Cell Biolabs) and comet DNA tail was considered level of DSB and analyzed by ImageJ software (OpenComet) (Sullivan-Reed et al., 2018). HR, D-NHEJ and Alt-NHEJ activities were measured by using DR-GFP (HR), EJ5-GFP (D-NHEJ) and EJ2-GFP (Alt-NHEJ) reporters (Bennardo et al., 2008; Pierce et al., 1999) as well as endonuclease I-SceI (Thermo Fisher Scientific) to generate double strand breaks in GFP cassette as described before (Nieborowska-Skorska et al., 2017b). Specific DSB repair activity was measured by detection of GFP+ cells.

Immunofluorescence

Cells were washed twice with 1X PBS before getting blocked by 1% bovine serum albumin (BSA) in 1X PBS together with human FC receptor block solution (Biolegend) in 10 minutes at RT. Primary anti-TGFβR1 (Santa Cruz Biotechnology) and anti-TGFβR2 (Invitrogen) antibodies were used and incubated at 4°C for 1 hour and followed by adding FITC-conjugated anti-mouse (for TGFβR1) and anti-rabbit (for TGFβR2) IgG antibodies (Invitrogen) also incubated at 4°C for 1 hour. To detect JAK2(V617F) kinase activity cells were fixed and permeabilized using a PerFix EXPOSE kit according to the manufacturer protocol (Beckman Coulter) followed by staining with anti-phosphotyrosine 4G10 mouse monoclonal antibody conjugated to FITC (Millipore). Cells were washed and re-suspended in 1X PBS before analyzing by flow cytometer and the output was visualized by FlowJo software (BD Biosciences, CA, USA).

Real-time RT-PCR

After incubating MV4-11 leukemia cells in BMM-dc condition with 10 μM SIS3 (Selleckchem) for 48 and 72 hours, RNA from cell lysate was isolated by TRI Reagent (Sigma Aldrich) and the Total RNA Mini columns (A&A Biotechnology). Then, 0.5 μg of total RNA was subjected to reverse transcription (RT) by M-MLV enzyme (Promega) with oligo dT (Bioline), random hexamers (Bioline) and RNase inhibitor (Blirt) in Promega buffer M-MLV diluted 5x in DEPC-treated water. The real-time RT-PCR master mix contained cDNA template (pre-diluted 2x in water), forward and reverse primers 0.5 μM each (listed in Table S2) and SensiFAST SYBR Green Hi-ROX reagent (Bioline) and the reaction was conducted in StepOnePlusTM Real-Time PCR System Thermocycler (Thermo Fisher Scientific).

The entire procedures followed the MIQE guidelines. To analyze real-time RT-PCR output, the difference in quantitative mRNA expression level was estimated by comparative ΔΔCt method and calculated as fold change ($2^{-\Delta\Delta Ct}$) with the expression level of 18SrRNAused for normalization.

ChIP

Cells were fixed in 1% formaldehyde for 15 minutes, and DNA was sonicated using a sonic dismembrator (Thermo Fisher Scientific) to generate 200–500-bp fragments. Chromatin was immunoprecipitated with anti-SMAD3 antibody (Cell Signaling Technology). ChIP-grade protein A/G magnetic beads (Pierce) were used for immunoprecipitation with antibody. Real- time PCR was performed with a master mix containing 1X Maxima SYBR Green, 0.25 μM primers and 1/50 of the ChIP DNA per well. Quantitative PCR reactions were carried out in triplicate using the ABI StepOnePlus PCR system. Data was normalized to DNA input. The primers are listed in Table S3.

Firefly/Renilla Luciferases transactivation assay

Gene specific promoter fragments containing putative SMAD3 binding sites and transcription start sites flanked by KpnI or XhoI restriction sites were generated by PCR using genomic DNA of the normal Lin-CD34+ human bone marrow cells. PCR was performed by using Q5 High-Fidelity DNA polymerase (New England Biolabs) and primers listed in Table S4. The Firefly luciferase reporter vectors were created by sub-cloning the gene-specific PCR fragments into the pGL3-basic vector (Promega) by KpnI and XhoI (Promega) restriction sites. All plasmids were analyzed and confirmed by restriction digestion and DNA sequencing. 293T cells were co-transfected with pGL4.73 (Renilla normalization vector), pGL3-Basic (Firefly reporter vector) containing gene specific promotor regions, and either with pMIG-empty or pMIG-SMAD3(WT) or pMIG-SMAD3(D407E) vectors using Lipofectamine 2000 (Invitrogen). Transfection efficiency was determined by detecting GFP+ cells (50%–60% of the total cell population). Luciferase activity was measured 60h after transfection. Samples were assayed for Firefly and Renilla luciferase activities using Dual-Glo Luciferase Assay System (Promega) and normalized according to the manufacturer instructions.

Gaussia Luciferase/Secreted Alkaline Phosphatase transactivation assay

$2x10^6$ of MV4-11 cells were transfected with 2 μg of pEZX-PG04.1 plasmids containing the indicated promoter fragments (GeneCopoeia) using Cell line Nucleofector kit V (Lonza) and Nucleofector 2b device (Lonza). Then the cells were suspended in the antibiotic-free growth medium and added to HS-5 cells (plated the preceding day) to start co-culture under hypoxia in the absence or presence of 10 μM SIS3 (Selleckchem). After 18h the activity of luciferase was detected in the cell culture conditioned medium immediately after collecting and assayed using Secrete-Pair Dual Luminescence Assay Kit (GeneCopoeia), following manufacturer protocol. Gaussia Luciferase (GL) activity (which transcription was under control of the studied promotor) was measured in GL-H buffer, assuring more sensitive detection. Bioluminescence signal generated by Secreted Alkaline Phosphatase (SEAP) expressed constitutively from the plasmid was measured in parallel for normalization. Luminescence was measured using the Promega Glomax 20/20 luminometer.

Detection of SMAD2/3/4 putative binding sites

These binding sites were detected in the genomic sequences downloaded from Ensembl using command line version of the program matrix-scan (quick) (Turatsinze et al., 2008) and the pre-computed first order (2-nt.) Markov-chain background models, based on both strands of the upstream noncoding regions of the genome, e.g., 2nt_upstream-noorf_Homo_sapiens_EnsEMBL-ovlp-2str for human. The motif scores are converted to p values, based on the distributions of scores computed for each motif using the program matrix-distrib. A uniform p value threshold of $p < 0.0001$ is used to call an instance of a particular motif at a given genomic position. The web service function PlotGenomic plots a graphical representation of selected NGD content in the ± 10 kb flank of the transcription start site of a chosen gene, and returns this content as tab-separated files. More precisely, this function returns instances of selected area types, and instances of selected motif types that intersect any of the returned area instances (Krystkowiak et al., 2013). We use a comprehensive set of transcription factor binding site (TFBS) motifs from several public motif libraries (Dabrowski et al., 2015).

MicroRNA quantification

hsa-183-5p, hsa-182-3p, hsa-103a-3p and UniSp6 miRNAs were examined in total cellular RNA enriched in miRNA, isolated from K562-wt, K562-Cr cells and from Lin^-CD34^+ FLT3(ITD);TET2mut AML cells treated with 10 μM SB431542 (Selleckchem) or vehicle using miRNeasy Micro Kit (QIAGEN). The same amounts of RNA were subjected to reverse transcription (performed in triplicates) followed by real-time PCR. Fold change in miRNA level relative to UniSp6 was calculated as $2^{-\Delta\Delta Ct}$.

Immunohistochemistry

GFP+ leukemia cells were visualized in formalin-fixed, peroxidases-quenched femoral bone marrow specimens of leukemia-bearing SCID mice by immunohistochemical staining according to standard methods. The sections of femoral bone marrow tissue were incubated with primary antibodies to anti-GFP (Invitrogen), immunodetection was performed using the Dako Envision+ polymer system and immunostaining was visualized with the chromogen 3, 3′-diaminobenzidine. Hematoxylin-counterstained sections

were viewed with a Nikon Eclipse 50i microscope and photomicrographs were taken with an attached Nikon DS-Fi1 camera (Melville, NY, USA).

QUANTIFICATION AND STATISTICAL ANALYSIS

All experiments were conducted at least in three independent replications. The mean and standard deviation (SD), and statistical analysis (p value) was executed by Student's t test in SigmaPlot (Systat software, CA, USA). Median survival time (MST) of mice was assessed by Kaplan-Meier log-rank test. Data are considered statistically significant when p value is less than 0.05.

Cell Reports, Volume *33*

Supplemental Information

TGFβR-SMAD3 Signaling Induces Resistance to PARP Inhibitors in the Bone Marrow Microenvironment

Bac Viet Le, Paulina Podszywalow-Bartnicka, Silvia Maifrede, Katherine Sullivan-Reed, Margaret Nieborowska-Skorska, Konstantin Golovine, Juo-Chin Yao, Reza Nejati, Kathy Q. Cai, Lisa Beatrice Caruso, Julian Swatler, Michal Dabrowski, Zhaorui Lian, Peter Valent, Elisabeth M. Paietta, Ross L. Levine, Hugo F. Fernandez, Martin S. Tallman, Mark R. Litzow, Jian Huang, Grant A. Challen, Daniel Link, Italo Tempera, Mariusz A. Wasik, Katarzyna Piwocka, and Tomasz Skorski

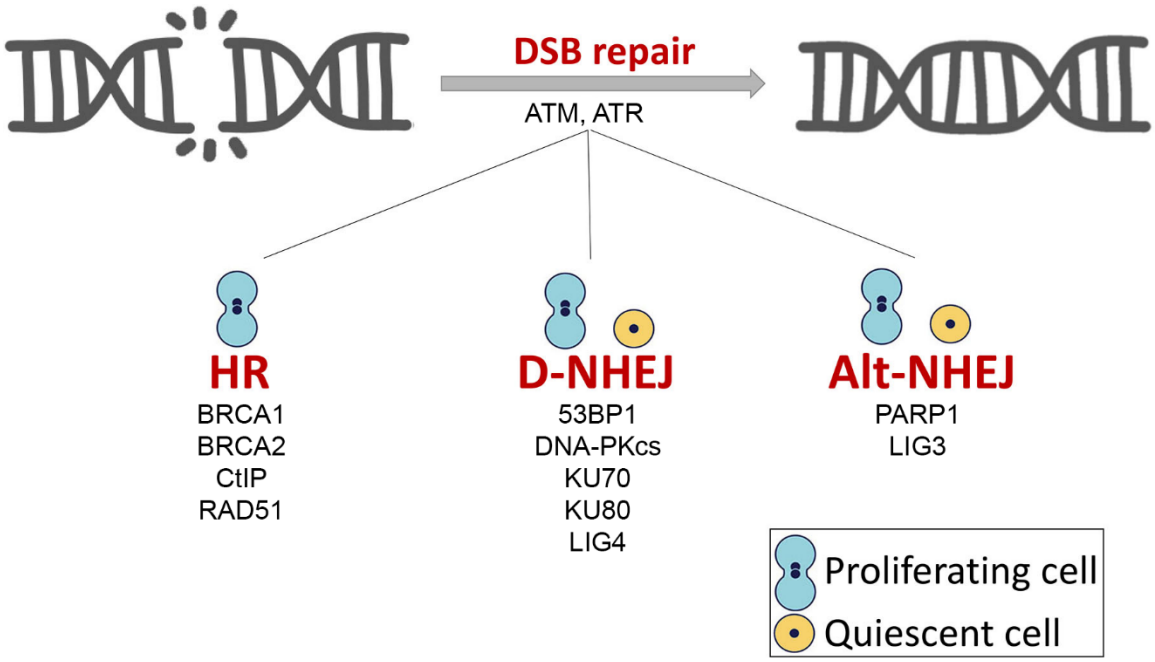

Figure S1; related to Figure 5. A diagram showing major DSB repair pathways in proliferating and quiescent cells.

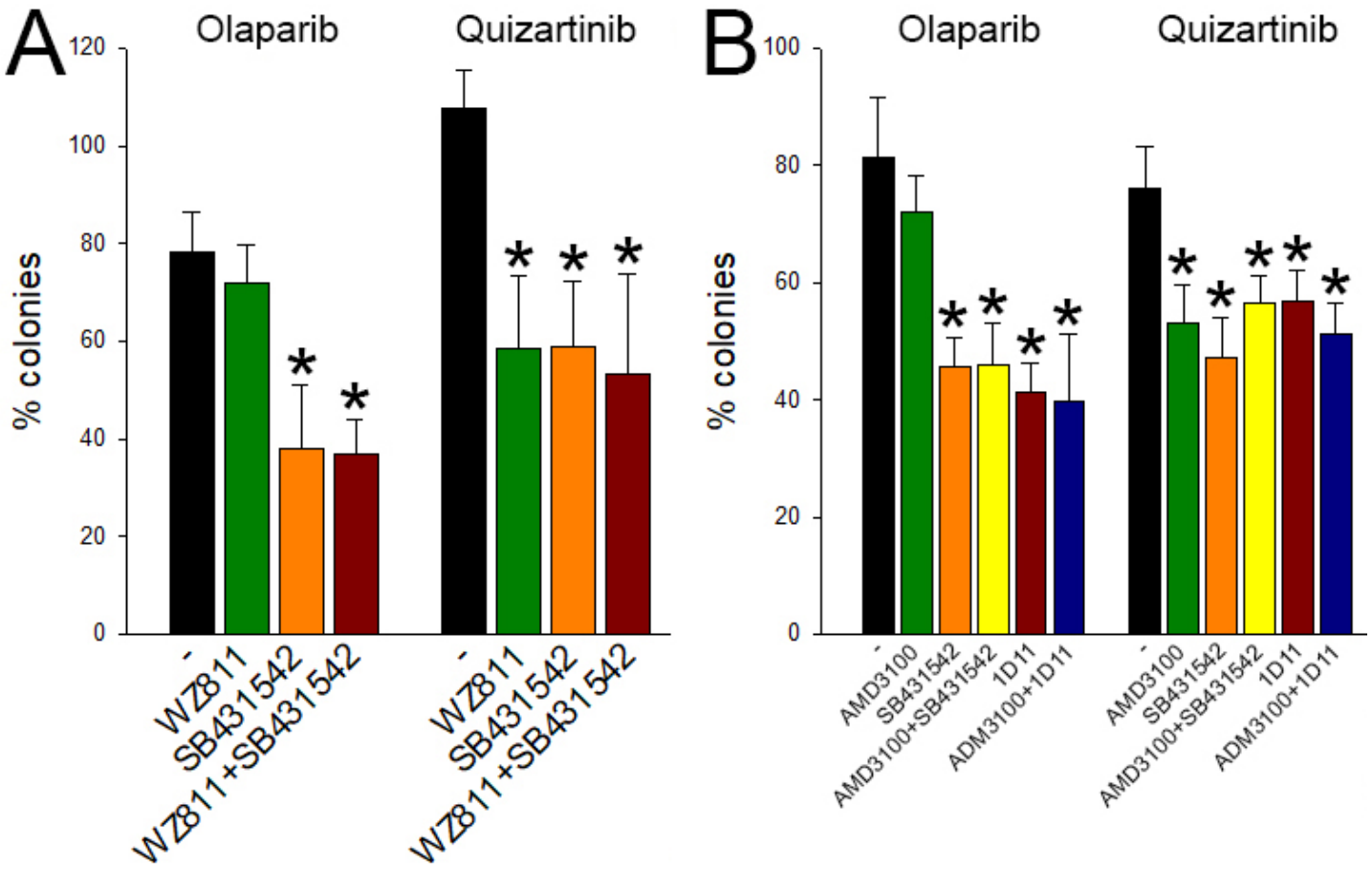

Figure S2; related to Figure 2. Role of TGF-β1-TGFβR and CXCL12 - CXCR4 signaling in regulating sensitivity of leukemia cells to PARPi and TKi in BMM. (**A**) Human FLT3(ITD);*TET2mut* Lin^-CD34^+ AML cells (3 patients) and (**B**) murine FLT3(ITD);*Tet2-/-* Lin^-cKit^+ AML-like cells (3 mice) were treated for 72 hrs in BMM-dc conditions with 1 μM olaparib or 100 nM quizartinib, and 10 μM TGFβR kinase inhibitor SB431542, 3 ng/ml TGF-β1 neutralizing antibody (1D11), 10 μM CXCR4 inhibitor AMD3100, 5 μM CXCR4 antagonist WZ811, or vehicle (-) followed by plating in methylcellulose. Results represent mean % ± SD (from 3 experiments) of colonies when compared to untreated cells; *$p<0.05$ when compared to untreated cells.

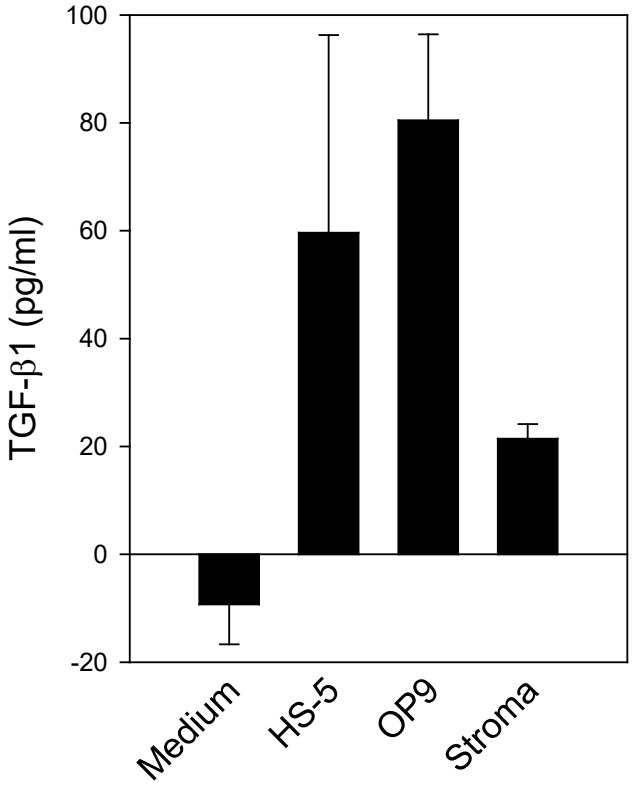

Figure S3; related to Figure 2. Stromal cells produce TGF-β1. Results represent mean concentration ± SD of TGF-β1 in serum-free conditioned medium from HS-5, OP9 and bone marrow stroma cells in serum-free medium.

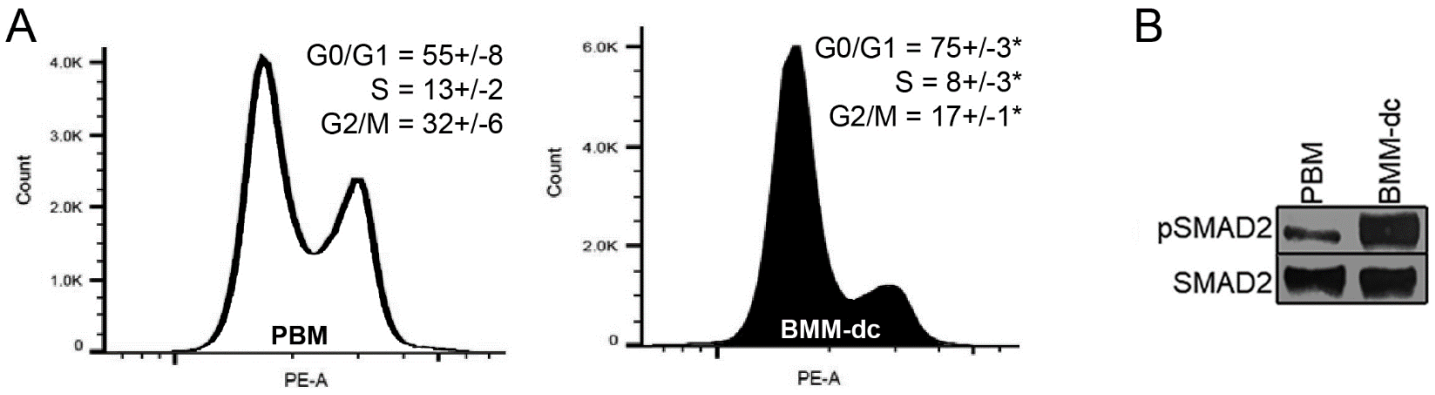

Figure S4; related to Figure 3. Inhibition of cell cycle in BMM. Human FLT3(ITD);*TET2mut* $Lin^{-}CD34^{+}$ AML cells were maintained in PBM or BMM-dc for 48 hrs. (**A**) Cell cycle analysis performed with propidium iodide. Results represent mean % of cells in cell cycle phases ± SD from triplicates; *$p<0.05$ when compared to PBM. (**B**) Western blot showing phospho-SMAD2 (pSMAD2) and SMAD2 in nuclear cell lysates.

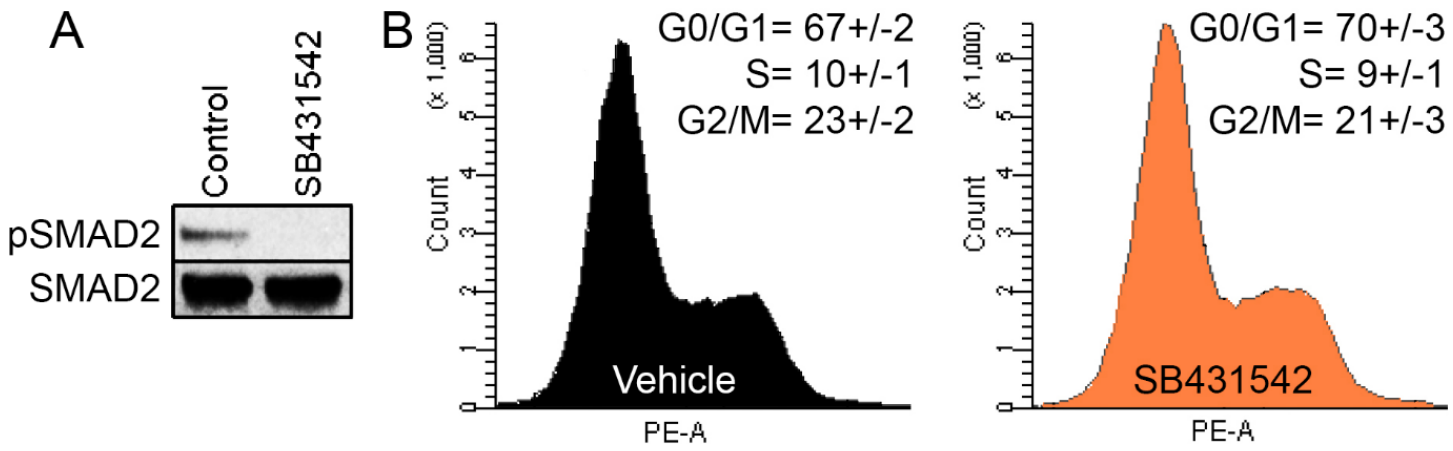

Figure S5; related to Figure 5. Inhibition of TGFβR kinase does not affect cell cycle progression of FLT3(ITD);*TET2mut* AML cells in BMM. Human FLT3(ITD);*TET2mut* $Lin^{-}CD34^{+}$ AML cells (3 patients) were treated for 48 hrs in BMM-dc with 10 μM TGFβR kinase inhibitor SB431542 or vehicle. (**A**) Western blot showing phospho-SMAD2 and SMAD2 in nuclear cell lysates. (**B**) Cell cycle analysis performed with propidium iodide. Results represent mean % ± SD from triplicates.

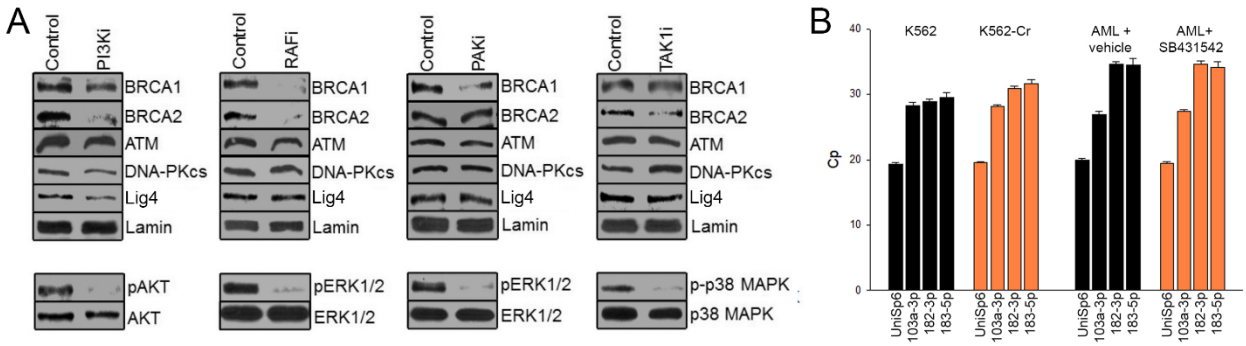

Figure S6; related to Figure 6. The role of PI3K, RAF, PAK and TAK1 kinases, and miRs 182 and 183 on the expression of DSB repair proteins in BMM. (**A**) Western analysis of the indicated proteins in murine FLT3(ITD);*Tet2-/-* cells treated for 72 hrs with 5 μM PI3Ki buparlisib, 2 μM RAF1i LY3009120, 5 μM PAK1i IPA-3, 10 μM TAK1i takinib or vehicle. The effect of specific inhibitors was confirmed by suppression of AKT, ERK1/2, and p38MAPK phosphorylation. (**B**) Expression levels of indicated miRNAs in K562-wt and TGFβR2-depleted K562-Cr cells, and $Lin^{-}CD34^{+}$ FLT3(ITD);*TET2mut* AML primary cells treated with 10 μM SB431542 or vehicle. Results show mean Cp value ± SD from 3 independent experiments, each run in 3 independent reverse transcription reactions and each reaction in duplicate. miR103a has been analyzed as control, a tumor-suppressor miRNA, which is changed in various cancers including myelodysplastic syndrome, however it is not located in the cluster with miR183/182 and its relation to TGF-β signaling is not documented.

Table S1. Primers used for mice genotyping; related to STAR Methods.

$Tet2^{fl/fl}$ FWD	AAG AAT TGC TAC AGG CCT GC
$Tet2^{fl/fl}$ REV	TTC TTT AGC CCT TGC TGA GC
PARP1 common	CAT GTT CGA TGG GAA AGT CCC
PARP1 wild-type	CCA GCG CAG CTC AGA GAA GCC A
PARP1 mutant	CAT GTT CGA TGG GAA AGT CCC
FLT3(ITD) common	TCT GGT TCC ATC CAT CTT CC
FLT3(ITD) wild-type	AGG AAG TCG ATG TTG GCA CT
FLT3(ITD) mutant	CTT CGT ATA ATG TAT GCT ATA CG
Vav-Cre FWD	AGA TGC CAG GAC ATC AGG AAC CT
Vav-Cre REV	ATC AGC CAC ACC AGA CAC AGA GAT C
JAK2(V617F) FWD	CGT GCA TAG TGT CTG TGG AAG TC
JAK2(V617F) REV	CGT GGA GAG TCT GTA AGG CTC AA
UBC-Cre FWD	GCA TTA CCG GTC GAT GCA ACG AGT GAT GAG
UBC-Cre REV	GAG TGA ACG AAC CTG GTC GAA ATC AGT GCG
$TGF\beta R2^{fl/fl}$ FWD	TAA ACA AGG TCC GGA GCC CA
$TGF\beta R2^{fl/fl}$ REV	ACT TCT GCA AGA GGT CCC CT

Table S2. Primers used for real-time RT-PCR; related to STAR Methods.

PRKDC FWD	CTG TGC AAC TTC ACT AAG TCC A
PRKDC REV	CAA TCT GAG GAC GAA TTG CCT
LIG4 FWD	AGC AAA AGT GGC TTA TAC GGA TG
LIG4 REV	TGA GTC CTA CAG AAG GAT CAT GC
ATM FWD	TTG ATC TTG TGC CTT GGC TAC
ATM REV	TAT GGT GTA CGT TCC CCA TGT
BRCA1 FWD	CAG AGG ACA ATG GCT TCC ATG
BRCA1 REV	CTA CAC TGT CCA ACA CCC ACT CTC
BRCA2 FWD	TTC AAA GAG CAA GGG CTG AC
BRCA2 REV	TGG GAA CAT TCC TTC CTA AGT CT
18SrRNA FWD	GTA ACC CGT TGA ACC CCA TT
18SrRNA REV	CCA TCC AAT CGG TAG TAG CG

Table S3. Primers used for quantitative PCR after ChIP; related to STAR Methods.

BRCA1 FWD Set 1	TTA TAT GCA CCA GTC AGC ACT C
BRCA1 REV Set 1	CCA AGT GCC CAC CAG ATT AG
BRCA1 FWD Set 5	GCC TTG GCG TCC ATT CT
BRCA1 REV Set 5	TCT CCC TCC ACA CTT CCC
ATM FWD Set 1	CCA CAG CAG GAA CCA CAA TA
ATM REV Set 1	CGA AAG AGG CGG GAC AAA
ATM FWD Set 2	GCG TGG CTA ACG GAG AAA
ATM REV Set 2	CTG CAC TCG GAA GGT CAA A
BRCA2 FWD Set 4	GCG CCT CGG GTG TCT TT
BRCA2 REV Set 4	GCT CCA GAG GTG CAG TTC TTT
PRKDC FWD Set 1	GCA GTC TCC TGA AAC CAT CTT A
PRKDC REV Set 1	ACT GCT CAC TTG CCA CTA TAT C
PRKDC FWD Set 2	GTG GTG GCT CAC ACC TAT AAT C
PRKDC REV Set 2	CAC TAT ATT GGT CAG GCT GCT ATC
LIG4 FWD Set 1	GAG CAG ACA AAG ACG CTA GAA
LIG4 REV Set 1	GAC TTT AGG CTT GGA GGG AAT TA

Table S4. Primers used for generation of transactivation reporters; related to STAR Methods.

ATM FWD	ACAGCT-ggtacc-CCACAGCAGGAACCACAATA
ATM REV	ACATCG-ctcgag-CTGCACTCGGAAGGTCAAA
BRCA1 FWD	ACATCG-ctcgag- ATCCACTCTCCCACGCCAGT
BRCA1 REV	ACAGCT-ggtacc-CCAAGTGCCCACCAGATTAG
BRCA2 FWD	ACAGCT-ggtacc-CACACTGAGAAATACCCGCAG
BRCA2 REV	ACATCG-ctcgag-GCTCCAGAGGTGCAGTTCTTT
PRKDC FWD	ACATCG-ctcgag-CTGCTCAGGACGCATTCCT
PRKDC REV	ACAGCT-ggtacc-CACTATATTGGTCAGGCTGCTATC
LIG4 FWD	ACATCG-ctcgag-GAGCAGACAAAGACGCTAGAA
LIG4 REV	ACAGCT-ggtacc- GACCCTAACCAGGATCCTGC